Earth Planets Space, **65**, 229–271, 2013

Infrared composition of the Large Magellanic Cloud

M. Siudek[1], A. Pollo[1,2,3], T. T. Takeuchi[4], Y. Ita[5], D. Kato[6*], and T. Onaka[7]

[1]*Center for Theoretical Physics of the Polish Academy of Sciences, Al. Lotnikow 32/46, 02-668 Warsaw, Poland*
[2]*Astronomical Observatory of the Jagiellonian University, Orla 171, 30-001 Cracow, Poland*
[3]*T National Centre for Nuclear Research, Hoza 69, 00-681 Warsaw, Poland*
[4]*Division of Particle and Astrophysical Science, Nagoya University, Furo-cho, Chikusa-ku, Nagoya 464-8602, Japan*
[5]*Astronomical Institute, Tohoku University, 6-3 Aramaki Aoba, Aoba-ku, Sendai, Miyagi 980-8578, Japan*
[6]*Institute of Space and Astronautical Science, Japan Aerospace Exploration Agency, 3-1-1, Yoshino-dai, Chuo-ku, Sagamihara, Kanagawa 252-5210, Japan*
[7]*Department of Astronomy, The University of Tokyo, Bunkyo-ku, Tokyo 113-0033, Japan*

(Received November 17, 2011; Revised September 2, 2012; Accepted September 3, 2012; Online published March 12, 2013)

The evolution of galaxies and the history of star formation in the Universe are among the most important topics in today's astrophysics. Especially, the role of small, irregular galaxies in the star-formation history of the Universe is not yet clear. Using the data from the AKARI IRC survey of the Large Magellanic Cloud at 3.2, 7, 11, 15, and 24 μm wavelengths, i.e., at the mid- and near-infrared, we have constructed a multiwavelength catalog containing data from a cross-correlation with a number of other databases at different wavelengths. We present the separation of different classes of stars in the LMC in color-color, and color-magnitude, diagrams, and analyze their contribution to the total LMC flux, related to point sources at different infrared wavelengths.
Key words: Large Magellanic Cloud, sky surveys, infrared, AKARI.

1. Introduction

Understanding the birth and evolution of galaxies is one of the most important problems of present-day extragalactic astrophysics. In order to study the early stages of galaxy evolution, it is crucial to understand the process of starformation in irregular galaxies with low metallicity, such as the Large Magellanic Cloud (LMC).

The irregular galaxies (Irr) are defined by their lack of organized optical structure (de Vaucouleurs and Freeman, 1972) and are the most common type of galaxy in the Universe (Hunter, 2002). In comparison with spiral galaxies they are, in general, smaller, less massive, less luminous and bluer (Gallagher and Hunter, 1984; Hunter and Gallagher, 1986). Irregular galaxies are simpler and are less dusty and lower in metallicity and shear in their interstellar mediums (Hunter and Elmegreen, 2004; Hunter, 2002) than spirals. In the context of chemical evolution, these galaxies are less evolved than spirals, as indicated by the high gas content and low abundances of heavy elements. That means that their interstellar medium was not in such a rate processed through stars (Hunter, 1997). Most Irr-type galaxies have on-going star formation and some are forming stars at rates normalized to their size that are comparable, or even higher, than those for spiral galaxies (Hunter, 1997; Gallagher and Hunter, 1984).

Irregular galaxies are an ideal laboratory to study various astrophysical processes influencing the evolution of large galaxies because their reaction to all internal or environmental perturbations, such as outbursts of supernovae or interactions with other galaxies, is stronger and occurs in shorter timescales due to their small dimensions and masses. Moreover, the absence of spiral density waves and a strikingly-different environment from that in spirals makes them useful for studying the star-formation process. Also, we believe that the first galaxies in the Universe were, in many aspects, similar to present-day irregular galaxies (Longair, 2008). Hence, the necessity to understand the evolution and star-formation histories of this type of galaxy.

The Large Magellanic Cloud (LMC) is an ideal laboratory to study molecular clouds, interstellar matter, gas and dust, and individual regions of star formation in the early stages of galaxy evolution, thanks to its favorable viewing angle (35°) (van der Marel and Cioni, 2001) and proximity (≈50 kpc) (Alves, 2004). Although LMC is sometimes classified as a one-armed spiral galaxy (according to de Vaucouleurs classification it is a very late type of a spiral galaxy, SB(s)m., i.e. an irregular spiral without a bulge) (Wilcots, 2009), the process of star formation is not limited to this particular structure, and we can treat it as a model for the star-formation process of irregular galaxies. A metal-poor environment ($Z \approx 0.3\ Z_{\odot}$) (Luck *et al.*, 1998), and a low dust-to-gas ratio (Koornneef, 1982) are responsible for its ultraviolet radiation field and chemical conditions of circumstellar materials (Shimonishi *et al.*, 2010). These characteristics may play a key role in the star-formation process of populous star clusters that have no galactic counter-

*Present address: Center for Low Carbon Society Strategy, Japan Science and Technology Agency, 7, Goban-cho, Chiyoda-ku, Tokyo 102-0076, Japan.

doi:10.5047/eps.2012.09.001

part (Fukui, 2005). Detailed studies of star formation in the LMC will enable an understanding of these processes.

In galaxies with an active star-formation process, the dominant source of dust are stars in the final stage of evolution (Asano *et al.*, 2013). The asymptotic giant branch (AGB) is an evolutionary phase of low- and intermediate-mass stars ($0.8\ M_{\odot} < M < 8M_{\odot}$) which actually expel gas and associated dust in the interstellar medium (ISM) via planetary nebula by superwind phenomena. Due to heavy mass loss and nucleosynthesis, AGB stars tend to be the dominant source of dust in the ISM (Groenewegen *et al.*, 2007).

Post-AGB stars are low- and intermediate-mass stars which rapidly evolve from the AGB towards the planetary nebula phase (this class includes planetary nebulae, PNe). Nowadays, there are a lot of unresolved questions about their evolution and physical processes, while nobody has constructed a complete theoretical model fitting their global properties. Within a group there is observed a large range of completely different photosphere abundance patterns, circumstellar geometries and kinematics. Moreover, their evolutionary phase is relatively short and the group of known post-AGBs is rather small. Post-AGB stars are characterized by a wide range of the electromagnetic spectrum. The central star is responsible for UV and optical emission, while the cool circumstellar envelope emits in the infrared (van Aarle *et al.*, 2009).

Studies of the LMC provide knowledge about young stellar objects (YSOs) which are a typical containment of stellar associations (star-forming stellar systems). There are strong correlations between young associations with one or more HII regions cataloged by Henize (1956) and Davies *et al.* (1976). Besides young bright stars there are a large amount of post-main sequence (PMS) stars (Gouliermis *et al.*, 2003; Nota *et al.*, 2006), whose distribution is correlated with molecular clouds. In the LMC, young associations younger than one million years are associated with the Giant Molecular Cloud (GMC) (Yamaguchi *et al.*, 2001; Fukui *et al.*, 2008). A correlation of ground-based, and Spitzer, observations of YSO candidates show that, in these regions, the star-formation process is active, and also a second generation of star formation occurs.

During the last decade, observing capability has increased, and there have been a lot of survey projects of the LMC at various wavelengths. Most studies have been made at ultraviolet (UV) and visible wavelengths, but observations in the infrared are crucial for investigating the formation and evolution of galaxies, because a significant fraction of the total emission falls in the infrared. Compared with optical-UV bands, the infrared is free of problems with dust absorption. Sensitive near-infrared surveys can derive information about the relative timescales of galaxy formation and point what controls the star-formation rate in galaxies. Ground-based near-infrared (NIR) surveys derive about fifteen million sources in the LMC (Kato *et al.*, 2007) but mid-infrared (MIR) surveys detect only a few thousand sources (Egan *et al.*, 2003), which is too shallow to compare with observations in other bands. Also the poorer angular resolutions of MIR surveys hamper a secure correlation with other catalogs. For the first time, the observations made by the Spitzer Space Telescope (SST) (Werner *et al.*, 2004), and AKARI, have a high spatial resolution. Moreover, the 11 and 15 μm wavelength bands are unique to AKARI.

Observations provided by the Spitzer Space Telescope Legacy Survey ("Surveying the Agents of a Galaxy's Evolution", SAGE) (Meixner *et al.*, 2006) have enabled studies of various astrophysical properties of evolved stars (Blum *et al.*, 2006; Hora *et al.*, 2008; Srinivasan *et al.*, 2009), young stellar objects (Whitney *et al.*, 2008), variables (Vijh *et al.*, 2009), and massive stars (Bonanos *et al.*, 2009). A SAGE catalog of massive stars with accurate spectral types and multiwavelengths in the Large Magellanic Cloud includes 1750 objects (Bonanos *et al.*, 2009). Analysis of color-magnitude diagrams shows that supergiant B[e], red supergiant, and luminous blue variable (LBV), stars are the dominant source of the LMC radiation at all infrared wavelengths (3.6, 4.5, 5.8, 8.0, 24.0 μm). SAGE-Spec Legacy Program obtained 52-93 μm spectra of 48 compact far-IR sources in the LMC, which were used for classification purposes (van Loon *et al.*, 2010). Analysis of the fine-structure lines of oxygen, (O I) at 63 μm and (O III) at 88 μm, enabled YSOs to be distinguished from evolved objects, and revealed new features about some objects in the LMC (van Loon *et al.*, 2010).

Within the program HERshel Inventory of The Agents of Galaxy Evolution (HERITAGE) observations of Magellanic Clouds performed by the Herschel Space Observatory's PACS and SPIRE cameras in 5 bands, 100, 160, 250, 350 and 500 μm, will be used to investigate the life cycle of matter (Meixner *et al.*, 2010). Far-infrared and submillimeter emission from dust grains have enabled the effective investigation of the dust from agents of galaxy evolution, which are the ISM, the most deeply-embedded YSOs, evolved massive stars, and supernovae (Meixner *et al.*, 2010). Maixner *et al.* (2010) constructed two dust models which fit the spectral energy distribution and reveal that 500 μm is in excess by 6% to 17%. The presented dust model, which uses amorphous carbon and silicate optical properties for Galactic dust, yields realistic gas mass ratios (GDR), consistent with prior observations. The model using standard graphite and silicate optical properties for Galactic dust is unrealistic for the LMC dust (Meixner *et al.*, 2010).

Observations in S11 and L15 data, which are unique to the AKARI survey, ensure new interesting features. AKARI data provided new information about mass-losing stars (Kato *et al.*, 2009; Onaka *et al.*, 2009) and enabled studies of stars with circumstellar dust (Ita *et al.*, 2009), the chemistry of the envelope (O- or C-rich), and the mass-loss rate accurately (Ita *et al.*, 2008). Ita *et al.* (2008, 2009) present new features on color-magnitude diagrams based on observations of an area of 10 deg^2 of the Large Magellanic Cloud using the onboard AKARI Infrared Camera. Color-magnitude diagrams achieved from 11 and 15 μm data revealed new information about dust emission, enabled stars with circumstellar dust to be identified, and show that oxygen-rich, and carbon-rich, giants become blue, and turn red again during their evolution.

In this Work, we present the results from a multiwavelength catalog, based on the AKARI 3 μm survey. Our catalog contains data from a cross-correlation with a number

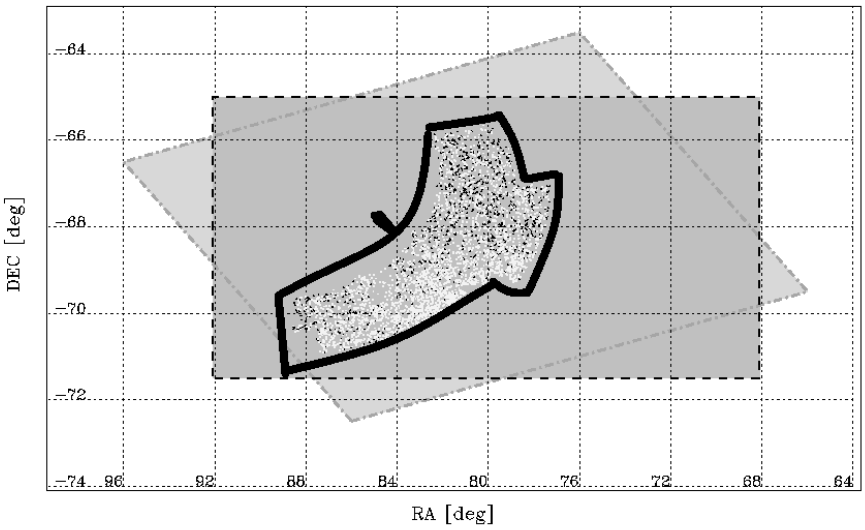

Fig. 1. AKARI observed an area of about 10 deg^2 of the Large Magellanic Cloud. The dash-dotted outline indicates the coverage of the Spitzer/SAGE survey (Meixner *et al.*, 2006), and the dashed outline shows the coverage of the Large Magellanic Cloud optical photometric survey (Zaritsky *et al.*, 2004). AKARI sources not identified in any of selected databases are shown with black triangles, and sources with identified counterparts by white squares.

of databases at different wavelengths. We show the separation of different classes of stars in the LMC in the color-magnitude, and color-color, diagrams and analyze the contribution of different classes of sources at different infrared wavelengths to the total LMC flux, related to point sources.

This paper is organized as follows: in Section 2, we show the basic information about the AKARI data: the sample with the complete color information. In Sections 3 and 4, we present and discuss how different types of objects separate in color-magnitude, and color-color, diagrams, respectively. In Section 7, we present the contribution from different objects to the total NIR and MIR flux in the LMC. We summarize in Section 8.

2. The Data

AKARI (ASTRO-F) is a Japanese infrared satellite launched on February 21, 2006 (Murakami *et al.*, 2007). AKARI has a lightweight telescope with a mirror of 68.5 cm effective diameter (Kawada *et al.*, 2007), and two onboard instruments: an Infrared Camera (IRC) (Onaka *et al.*, 2007) and a far-infrared surveyor (FIS) (Kawada *et al.*, 2007). Both instruments have a high-spatial-resolution/low-to-moderate-resolution spectroscopic capability. IRC has three independent channels: NIR (1.8–5.5 μm), MIR-S (4.6–13.4 μm), and MIR-L (12.6–26.5 μm), nine imaging bands (three for channel) and six dispersion elements (two for channel). NIR and MIR-S channels observed the same field of view due to the focal-plane layout, while MIR-L observed a field shifted by 25′ with respect to the NIR/MIR-S center in a direction perpendicular to AKARI's orbit. Each channel has a wide field of view of about 10′ × 10′, and adjacent fields overlap by 1.5′. The photometry was independently performed for each of the pointed observations. Therefore, all sources that fall in the overlapping regions between adjacent Fields of View (FOVs) have more than one photometric measurement. In those cases, only the source with the best signal-to-noise (S/N) was listed in the catalog, and the other(s) were abandoned.

AKARI has carried out two large-area legacy surveys: one of them was the LMC survey project (PI. T. Onaka) in the pointing mode. To map the LMC effectively, observations were performed during three separate seasons, from May 6, 2006, to June 8, 2006, from October 2, 2006, to December 31, 2006, and from March 24, 2007, to July 2, 2007. As a positional reference, the Two Micron All-Sky Survey (2MASS) catalog (Skrutskie *et al.*, 2006) was used. At least five matched point sources were used to compute the coordinate transform matrix that relates the image pixel coordinates to the sky coordinates. When sources were not found in 2MASS, transformation from the image pixel coordinates to the sky coordinates was based on matching detected sources with the SAGE point source catalog (Meixner *et al.*, 2006). The root-mean-squares of the residuals between the input 2MASS SAGE catalog coordinates, and the fitted coordinates, are smaller than 1:2, 2:6, and 2:9, for NIR, MIR-S, and MIR-L images, respectively (Ita *et al.*, 2008).

Bearing the above-mentioned observing strategy in mind, we should note that simultaneous observations of variable stars in different photometric bands are very important for constructing their correct infrared spectral energy distributions (SEDs) and for placing them correctly in color-magnitude, and color-color, diagrams. Due to intervals in observational time, the location of variable stars on color-color, and color-magnitude, diagrams will be biased by an additional scatter, because of changes in amplitudes and phases of variability. This effect has to be taken into account when interpreting color-color, and color-magnitude, diagrams of variable stars.

Observations of the LMC were carried out using IRC with wavelengths of N3 (3.2 μm), S7 (7.0 μm), S11 (11.0 μm), L15 (15.0 μm), L24 (24.0 μm), and a dispersion prism (2–5 μm, $\lambda/\delta\lambda \approx 20$). For the first time, observa-

tions were carried out with imaging filters S11 and L15. These properties make the AKARI IRC unique, and complementary to the instruments onboard the Spitzer Space Telescope. The NIR camera covers band N3, which can provide new information about carbon-rich objects. The AKARI IRC N3 filter is slightly bluer than the IRAC [3.6] filter, it covers the range from 2.7–3.8 μm, while IRAC on board SST covers the range 3.15–3.90 μm. Ita *et al*. (2008) found new features of certain types of stars, comparing N3 and [3.6] photometries. Thanks to the higher sensitivity to the 3.1 μm HCN + C_2H_2 absorption of the N3 filter, than that of the [3.6] passband, observations in the N3 band are useful for identifying carbon-rich stars.

The entire LMC was also mapped by AKARI as part of the All-Sky survey at 6 bands in the mid- to far-infrared wavelengths (Ishihara *et al*., 2006; Kawada *et al*., 2007) in 4 bands between 50 and 180 μm. Due to multiband (11 bands) observations, AKARI provides a new window for studying star formation and galaxy evolution. The LMC survey carried out over 600 pointing observations with IRC during three seasons from May 2006 to July 2007.

Observations over an area of about 10 deg^2 of the LMC were performed in a pointing opportunity, in which the telescope was pointed at a given position for about 10 min. There were detected over 5.9×10^5, 8.8×10^4, 6.4×10^4, 2.8×10^4, and 1.5×10^4 point sources at N3, S7, S11, L15, L24 bands, respectively (Ita *et al*., 2008; Kato *et al*., 2009). In comparison, the Spitzer SAGE project detected only about 2×10^5 sources over an area of about 49 deg^2 of the LMC with all IRAC bands at two epochs separated by 3 months (Fazio *et al*., 2004). The Release Candidate version 1 (hereafter RC1) of the AKARI LMC Large Area Survey point source catalog contains about a million sources (Ita *et al*., 2008; Kato *et al*., in prep). The fluxes for zero magnitude for the five IRC bands are 343.34, 74.956, 38.258, 16.034, and 8.0459 Jy (Tanabé *et al*., 2008). The 10-sigma limiting magnitudes are 16.8, 13.4, 11.5, 9.9 and 8.5 mag at N3, S7, S11, L15, and L24, respectively, and the 90% completeness limits are 14.6, 13.4, 12.6, 10.7, and 9.3 mag at N3, S7, S11, L15, and L24, respectively (see Table 1).

RC1 includes two different sets of data:

- Catalogs—including only reliable sources, i.e. sources matched with a Spitzer/SAGE source within a radius of 3 arcsec (Meixner *et al*., 2006).
- Archive—including sources with a low reliability or large photometric uncertainties (all detected sources).

As Archive should be used with caution, we based our first analysis on sources from Catalogs. This data set contains 754 288 sources, but only 7 722 were detected in L24 wavelength.

For the first analysis, we selected from Catalogs all sources (3 852) detected at all NIR and MIR wavelengths of: 3.2, 7.0, 11.0, 15.0, 24.0 μm, i.e. with a complete five-band color information. This sample of data was used to create color-magnitude, and color-color, diagrams presented in Sections 4 and 3, and an analysis of contributions from different objects to the total NIR and MIR flux in the LMC presented in Section 7.

In order to identify and classify sources, we searched for counterparts of selected sources based on the AKARI 3 μm survey in publicly-available databases at different wavelengths: 2MASS (Cutri *et al*., 2003; Skrutskie *et al*., 2003; Karachentseva *et al*., 2010), NED, SIMBAD, AKARI FIS All-Sky Survey (Yamamura *et al*., 2010), OGLE (Soszyński *et al*., 2008a, b, 2009a, b, c; Poleski *et al*., 2010a, b). We cross-correlated our sources with these catalogs using a positional tolerance of 3.0 arcsec, extended to 20 arcsec for the cross-correlation only with the AKARI-FIS data. If more than one object was found within the tolerance circle, the closest one was chosen. For almost 75% of the sample (2 836 from 3 852 sources), counterparts were found. In Fig. 1, a spatial distribution of identified and unidentified sources in the LMC is shown. Sources without a counterpart within a tolerance circle (1 016) should be further investigated. Such sources can be stars which are invisible due to a large amount of surrounding dust (e.g. OH/IR stars, dusty carbon stars, etc.).

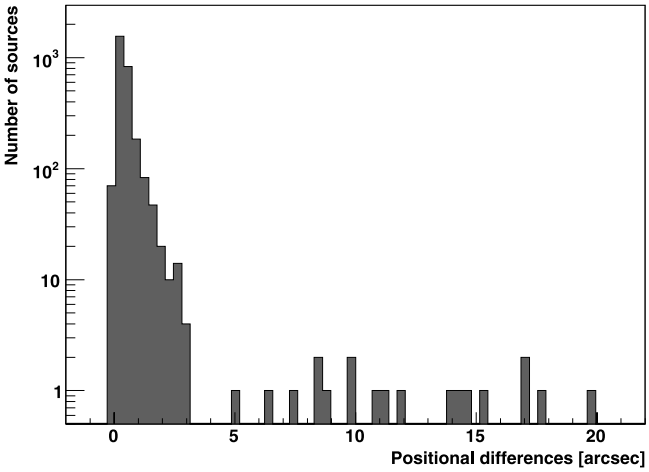

Fig. 2. The distribution of positional differences between the sources and identified counterparts. The size of the bin is 0.3 arcsec.

In Fig. 2, a distribution of positional differences for matched sources (2 836) is shown. The mean positional difference is 0.57 arcsec, however a mean is not adequate for our sample due to an extension of positional tolerance to 20 arcsec for cross-correlation with the AKARI-FIS data. The median value of the positional difference is 0.41 arcsec. Figure A.1 (see Appendix A) shows a distribution of positional differences for matched sources only, with 2MASS, NED, SIMBAD, AKARI FIS All-Sky Survey, OGLE counterparts, respectively.

We have found the largest amount of matches by cross-correlation of AKARI sources with 2MASS (2 661). Slightly fewer counterparts were identified in SIMBAD (2 233). With a tolerance radius of 3.0 arcsec, we have found 1 506 matches between AKARI sources and OGLE. By a cross-correlation with NED, we have identified only 244 objects. Although we have extended a positional difference to 20 arcsec for AKARI-FIS data only 77 sources were found. For about 35% of sources (1 370), counterparts were found in all used databases excluding AKARI FIS All-Sky Survey and NED databases. Most of the counterparts were identified in 2MASS and SIMBAD, and for 1 389

Table 1. Survey properties.

Properties	N3	S7	S11	L15	L24
Channel	NIR	MIR-S	MIR-S	MIR-L	MIR-L
Reference wavelength [μm]	3.2	7.0	11.0	15.0	24.0
10 σ detection limit [mag]	16.8	13.4	11.5	9.9	8.5
Saturation limit [mJy]	250	1800	1800	2500	23000
Saturation limit [mag][a]	7.8	4.0	3.3	2.0	-1.1
Zero magnitude limits[b]	343.34	74.956	38.258	16.034	8.0459
90% completeness limits [mag]	14.6	13.4	12.6	10.7	9.3
Number of detected sources (Ita *et al.*, 2008)	$> 5.9 \times 10^5$	$> 8.8 \times 10^4$	$> 6.4 \times 10^4$	$> 2.8 \times 10^4$	$> 1.5 \times 10^4$
Number of sources in RC1 – Archive	$> 8.7 \times 10^5$	$> 18.7 \times 10^4$	$> 14.7 \times 10^4$	$> 11.1 \times 10^4$	$> 16.1 \times 10^4$
Number of sources in RC1 – Catalog	$> 7.5 \times 10^5$	$> 10.6 \times 10^4$	$> 6.4 \times 10^4$	$> 2.8 \times 10^4$	$> 0.77 \times 10^4$

[a] Numbers are taken from ASTRO-F Observer's Manual version 3.2.[2].
[b] Tanabé *et al.* (2008).

sources the same object was identified in both databases. In some cases, we have identified sources only in one of the databases. We have found 525 matches in the tolerance radius only between AKARI sources and 2MASS. 117 AKARI sources were identified only in SIMBAD. For 9 sources, counterparts were found only in NED. With cross-correlation with AKARI-FIS data, we have found counterparts for 20 sources, and only for 2 with cross-matching solely with OGLE.

For sources with identified counterparts (2 836), we compiled all the available information about types of objects from all the databases. Within our sample we have found 1 964 objects (51% of the sample) with a more detailed source type. If more than one object type was found for a single source we gathered all information, and if the types were different we have mostly followed the SIMBAD classification. We distinguish the following categories of objects:

- AGB stars, including objects classified as AGBs, candidates for AGB, carbon stars, or Mira stars.
- other possible late-type pulsating giants (possible AGBs or similar), including objects classified as variable stars, stars suspected of variability, semiregular variables (SRVs), or OGLE small amplitude red giants (OSARGs).
- post-AGB stars, including objects classified as Planetary Nebula or possible Planetary Nebula.
- Young stellar objects, including objects classified as YSOs or candidates for YSO.
- multiple systems, including objects classified as stars in a cluster, stars in association, multiple objects, clusters of stars or double or multiple stars.
- sources of unknown origin, including objects classified as Radio-/ IR-/ UV-/ X-/Red-sources.
- background objects, classified as galaxies, quasi-stellar objects (QSOs) or active galactic nucleus (AGNs).
- foreground objects, classified as objects known to be placed within the Milky Way Galaxy.
- others, including one of the remaining objects with an identified type but not included in the above categories.

In Fig. 3, a spatial distribution of different categories of objects in the Large Magellanic Cloud is shown.

Among the identified sources, candidates for AGB stars dominate and amount to 42% of the objects of identified types. If classification is tentative, they are classified as other late-type pulsating giants (27% of the sample), which means that if these objects are not exactly AGBs, they are pulsating red giants not so far removed from AGBs in their evolutionary and physical properties. More than 6.7% of the selected group are background objects, mainly galaxies (about 6.5%). We also found a group of young stellar objects (3.6%), multiple systems (2.5%), post-AGBs (2.0%) and others, of which mostly are related to stars. Within the sample, only 4 objects identified as Galactic sources were found, however in our sample there are probably more Milky Way objects.

The effect of unequal Galactic foreground extinction, as well as that of the local interstellar extinction, due to the LMC disk material, should also be analyzed carefully, particularly for N3 band data. Based on Sakon *et al.* (2006), the Galactic foreground emission at COBE DIRBE bands range from 3.6 to 7.5 MJy/sr at 100 μm and from 6.4 to 14.7 MJy/sr at 140 μm, assuming a correlation between the HI and infrared emissions within the AKARI LMC Large Area survey area, where the Galactic HI intensity ranges from 300–600 K km/s. The optical depth at 100 μm can be estimated as $\tau(100\ \mu\text{m})=2.4\cdot10^{-4}$–$7.2\cdot10^{-4}$. In this case, the effect of Galactic foreground extinction variations on the N3 band strength of sources within the observed area must be smaller than a few percent even if $A_{\rm N3}/\tau(100\mu\,\text{m}) \approx 30$ is assumed (Sakon *et al.*, 2006).

A discussion of foreground and background objects is presented in Section 5. The fractions of different types of objects among IR-bright LMC sources are shown in Table B.1. The properties of AGB, other late-type pulsating giants, and post-AGB stars are summarized in Table C.1.

There remains a possibility of misidentification, since the gathered data are compilations of data from several databases. However, a few possible misidentifications should not affect the final result of this Work.

3. Color-Magnitude Diagrams

Color-magnitude diagrams are a tool often used in astronomy and often show a clear separation of different ob-

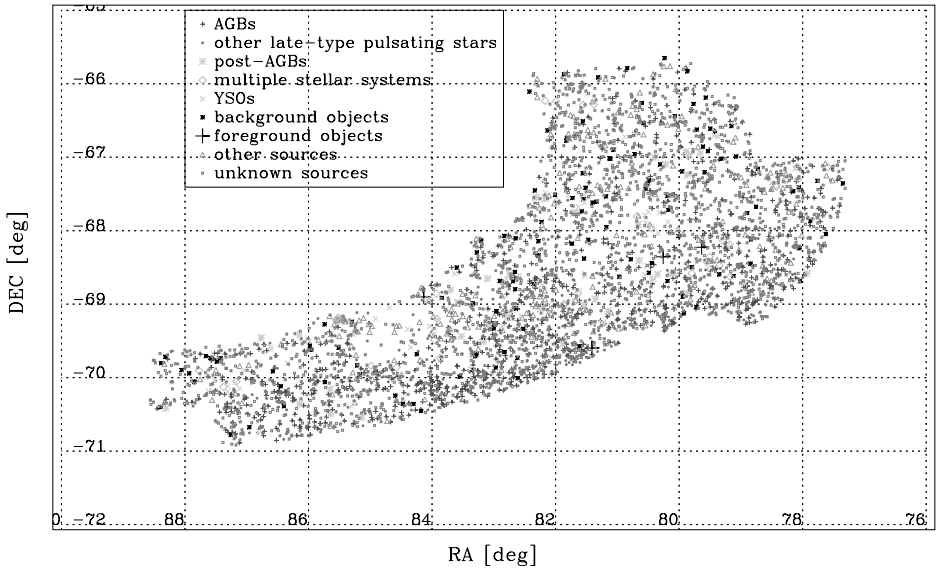

Fig. 3. Spatial distribution of different sources. AGB stars are shown as small plus signs, other late-type pulsating giants as gray filled circles, post-AGB stars as asterisks, multiple stellar systems as gray diamonds, YSOs as gray X signs, background objects as black asterisks, foreground objects as gray plus signs, other sources as triangles, and unknown sources small, open squares.

jects. Infrared color-magnitude diagrams have been often used for the analysis of Spitzer/SAGE data (Blum *et al*., 2006; Meixner *et al*., 2006; Bonanos *et al*., 2009). Adding S11 and L15 data (unique to the AKARI survey) ensures additional new features and can be essential for the estimation of the silicate band strength in mass-losing stars (Kato *et al*., 2009; Onaka *et al*., 2009). Color-magnitude diagrams have been used to identify stars with circumstellar dust and to show that dust emission is related, not only to sources brighter than the tip of the first red giant branch, but also to fainter red giants (Ita *et al*., 2009). Ita *et al*. (2009) correlates this new sequence with red giants with aluminum oxide dust without the silicate feature. IRC limits enable detection only to the brightest end of the YSOs—stars such as T Tauri are too deep for AKARI IRC survey—although young stars of intermediate mass (Herbig Ae/Be), or classical Be stars can be almost completely detected. IRC is capable of detecting all mass-losing AGB stars (Ita *et al*., 2008). The N3 band is sensitive to the 3.1 μm $HCN+C_2H_2$ absorption feature. This absorption line is a characteristic of carbon-rich AGB stars (e.g, van Loon *et al*., 1999) but can also be attributed to water ice (Manteiga *et al*., 2011). On the basis of the N3 color, it is possible to determine which sources are carbon-rich. Observations in the S11, L15, L24 bands can ensure information about the chemistry of the envelope (O- or C-rich), and the mass-loss rate accurately, thanks to the presence of silicate bands at 10 and 18 μm, and the silicon carbide band at 11.3 μm (Ita *et al*., 2008).

In this section, we analyze color-magnitude diagrams with all different types of sources (Section 3.1), and we also make further comparison of only AGB and post-AGB stars (Section 3.2). The distributions of the photometric uncertainty versus the magnitude in the IRC bands for selected sources are shown in Fig. 4. More about the accuracy of the photometry for all the samples can be found in Ita *et al*. (2008). More information about the IRC imaging data pipeline can be found in the IRC Data User's Manual[1]. Photometric uncertainty for our sample remains negligible when we analyze color-color, and color-magnitude, diagrams. However, differences in phase may play a role in creating a dispersion of the properties of variable stars in these plots.

3.1 Separation of different types of sources in color-magnitude diagrams

In order to analyze color-magnitude diagrams, we discriminated among our sample following groups of objects:

(1) AGB stars (including sources classified as: AGBs, candidates for AGBs, carbon stars, or Mira stars);
(2) other possible late-type pulsating giants;
(3) post-AGB stars, mainly Planetary Nebulae and protoplanetary nebulae;
(4) multiple stellar systems;
(5) YSOs;
(6) background objects; and
(7) foreground objects.

Color-magnitude diagrams of different types of sources from our sample are shown in Fig. 5. In all the color-magnitude diagrams, different types of objects are well separated, there is an especially prominent separation between a group consisting of multiple stellar systems, possible late-type pulsating giants, AGB stars, and foreground objects, and a group including YSOs, post-AGB stars and background objects, as is clearly shown in Fig. 5. As shown in diagram N3–S7 vs. N3 (upper panel of Fig. 5) post-AGB stars, YSOs, and background objects, are among the least luminous stars at 3.2 μm. The most luminous groups are multiple stellar systems. Also a group of other late-type giants tend to be among the most luminous stars at 3.2 μm, but this group is nonuniform and objects are spread over the whole diagram. AGB stars are less luminous than multi-

[1] http://www.ir.isas.jaxa.jp/ASTRO-F/Observation/#IDUM.

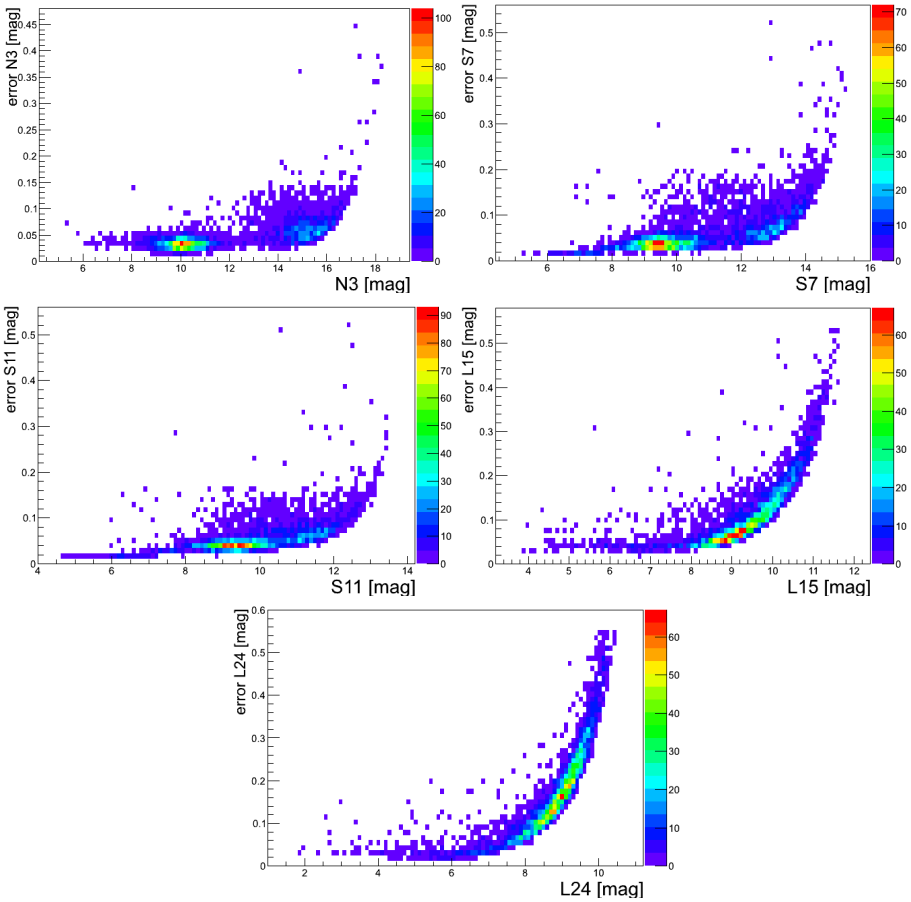

Fig. 4. Photometric uncertainties as a function of the magnitude at each IRC band for sources with full color information.

ple stellar systems, but they are significantly more luminous than YSOs and post-AGB stars. AGB stars, other late-type pulsating giants, multiple stellar systems, and foreground objects, occupy the "bluer" part of the color-magnitude diagrams and YSOs, post-AGB stars, and background objects, tend to be found in the "redder" part. YSOs tend to occupy the "reddest" part of the diagrams, while post-AGB stars and background objects are scattered. AGB stars form a large cloud in the "bluer" part of the diagram, with a long tail going into the "redder" part. Due to a small amount of foreground objects, they are not well separated but they are placed in the "bluer" regions and are similar to, or more luminous than, AGB stars.

Post-AGB stars and background objects also tend to be the least luminous at 7.0 μm, which is visible in the diagram N3–L24 vs. S7 (middle panel of Fig. 5), but the luminosity of YSOs is comparable to the luminosity of AGB-stars. Also, multiple objects have a similar tendency as in 3.2 μm and they are among the most luminous stars, but, at 7.0 μm, some AGB stars also tend to be among the most luminous objects. YSOs and post-AGBs are "redder" than AGB stars and possible AGBs or similar giants. At 11 μm it is not clear what kind of objects are the most luminous because each group spans quite a wide range of luminosity. In the N3–S11 vs. S11 diagram (lower panel of Fig. 5) a tendency to form clouds by all groups stretching from a lower to a higher luminosity is visible. Most of the multiple objects and AGBs represent luminosities similar to the background objects, which are less luminous than YSOs. Yet, AGB stars, pulsating giants and multiple systems are well separated from post-AGB stars, YSOs and background objects. Multiple stellar systems, foreground objects, and AGB stars, occupy the "bluer" part of the diagram, while YSOs, post-AGB stars, and background objects, are found in the "redder" part. At 15.0 and 24.0 μm, all different types of objects are widely spread over the luminosity range and it is hard to distinguish the most luminous group.

3.2 Separation of AGB and post-AGB stars in color-magnitude diagrams

In this section, we discuss the color-magnitude diagrams of AGBs, other late-type pulsating stars possibly being AGBs, or close to the AGB phase, and post-AGBs (groups (1), (2), and (3) from 3.1). We divide the sources into the following types:

(a) post-AGB stars (including Planetary Nebulae);
(b) Mira stars;
(c) carbon stars;
(d) candidates for AGB stars (including sources which probably are AGB stars but their type was not confirmed);
(e) variable stars;
(f) semiregular variables (SRVs); and
(g) OGLE small amplitude red giants (OSARGs).

Color-magnitude diagrams for the AGB group are presented in Fig. 6. In all color-magnitude diagrams, different types

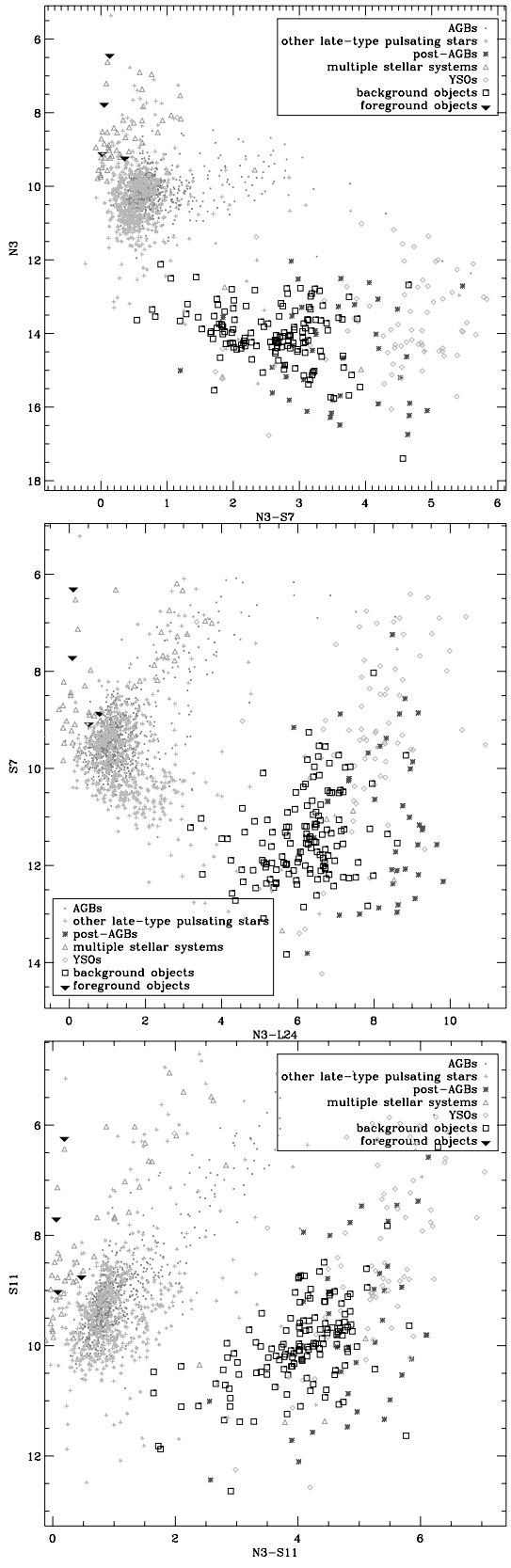

Fig. 5. Position of different types of objects in the color-magnitude diagrams N3–S7 vs. N3 (upper), N3–L24 vs. S7 (middle), N3–S11 vs. S11 (lower). AGB stars are shown as small gray filled circles, other late-type pulsating giants as gray plus signs, post-AGB stars as asterisks, multiple stellar systems as gray open triangles, YSOs as gray diamonds, background objects as black open squares, and foreground objects as black filled triangles.

are well separated. Post-AGB stars, especially, form a separate group in the "redder" regions of the diagrams. Also, Mira stars tend to form a compact, clear separated cloud in the "bluer" part of the diagrams, especially in diagram N3–L24 vs. N3 (upper panel of Fig. 6), and S11–L24 vs. L24 (lower panel of Fig. 6). As shown in diagram N3–L24 vs. N3 (upper panel of Fig. 6), a group of (e) variable stars, (f) SRVs, and (g) OSARGs, are among the most luminous stars at 3.2 μm, and post-AGB stars are among the least luminous objects. Variable stars do not seem to form any separate cloud, they are spread over the whole diagram. As shown in diagram N3–L24 vs. S7 (middle panel of Fig. 6), SRVs, a small group of variable stars, are among the most luminous stars, not only at 3.2 μm but also at 7 μm, but also in this band Mira stars tend to have similar luminosities. Post-AGB stars, as at 3.2 μm, are also among the least luminous objects at 7 μm, and they occupy the "redder" part of the diagram. However, post-AGB stars tend to be more luminous than carbon stars and AGB stars at 24 μm, although a group of post-AGBs are quite widely spread in luminosity.

Color-magnitude diagrams presented by Ita *et al.* (2008) show a clear separation in luminosity and color between carbon stars, dusty red giants and YSO candidates. Since Ita *et al.* (2008) estimate the absolute magnitude by adding the distance modulus to the observed magnitude, and we do not, a straightforward comparison of our diagrams with those of Ita *et al.* (2008) is not possible.

Moreover, our sample is different. Ita *et al.* (2008) based their analysis on all detected sources, i.e. over 5.9×10^5, 8.8×10^4, 6.4×10^4, 2.8×10^4, and 1.5×10^4, point sources at the N3, S7, S11, L15, L24, bands, respectively. Our work is based only on reliable data provided by RC1 with full color information. A comparison of the number of sources used by Ita *et al.* (2008), and in this paper, is presented in Table 1.

YSO candidates have redder colors than other groups, both in our, and the Ita *et al.* (2008), color-magnitude diagrams. Also, color-magnitude diagrams with Spitzer data show that YSOs are among the reddest objects (Meixner *et al.*, 2006). In the mid-infrared diagrams presented by Ita *et al.* (2008), dusty red giants are brighter than optical carbon stars. As we have divided our sample into different categories of types it is not easy to verify this information. However, in our infrared color-magnitude diagrams, Mira stars are more luminous than carbon stars. Observations in the N3 band, thanks to the sensitivity to 3.1 μm HCN + C_2H_2, could be useful for separating carbon-rich AGBs on the basis of their colors.

4. Color-Color Diagrams

As was discussed in Section 3, color-magnitude diagrams can be used to distinguish different types of objects. Also color-color diagrams give us useful information about the properties of different objects. As in the previous section, we analyze color-color diagrams with all different types of sources (Section 4.1). In Section 4.2, we present a further comparison of the group of AGB and post-AGB stars.

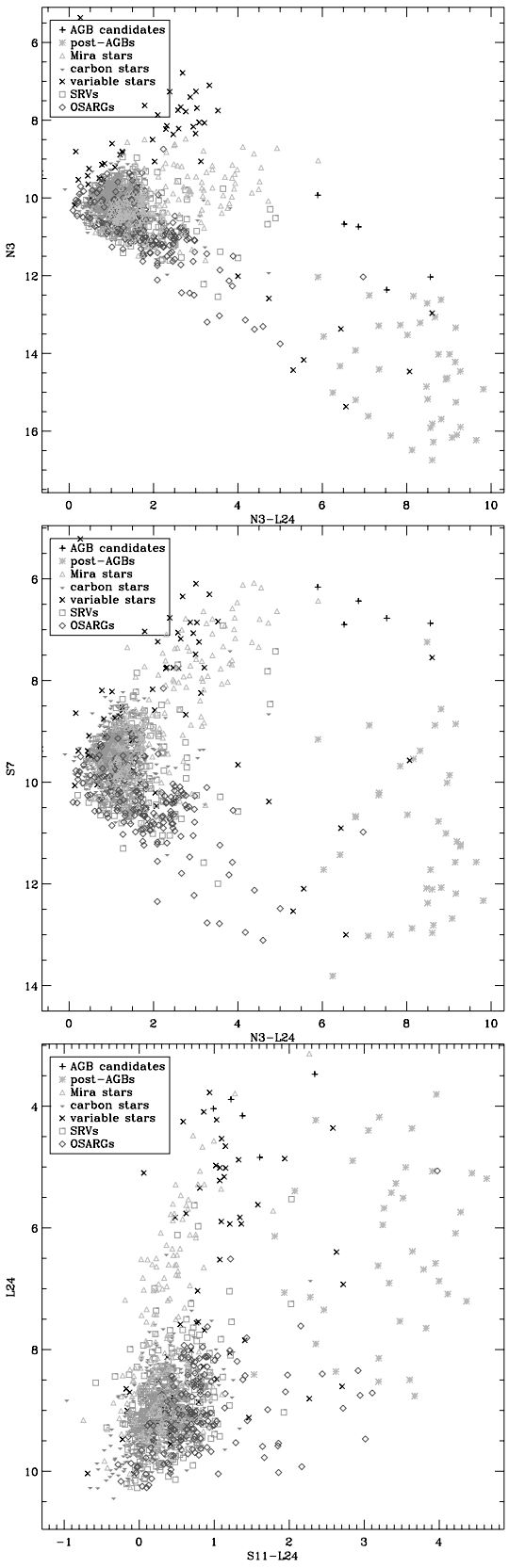

Fig. 6. Position of different types of objects in the color-magnitude diagrams N3–L24 vs. N3 (upper), N3–L24 vs. S7 (middle), S11–L24 vs. L24 (lower). (d) AGB candidates are shown as plus signs, (a) post-AGB stars as gray asterisks, (b) Mira stars as gray open triangles, (c) carbon stars as black filled triangles, (e) variable stars as X signs, (f) SRVs as gray open squares, and (g) OSARGs as diamonds.

4.1 Separation of different types of sources in color-color diagrams

As in Section 3.1, we divide classified sources into groups of: (1) AGB stars, (2) other late-type pulsating giants, (3) post-AGB stars, (4) multiple stellar systems, (5) YSOs, (6) background objects, (7) foreground objects. Color-color diagrams of the different types of sources from our sample are shown in Fig. 7.

In all color-color diagrams different types are well separated. Especially, AGB stars and YSOs tend to occupy separate parts of the diagrams. YSOs and post-AGB stars are significantly "redder" than most AGB stars or possible AGB stars, which is visible on all diagrams. AGB stars with other late-type pulsating giants shows a rather clear pattern on all color-color diagrams with a tendency to occupy the "bluer" parts of the diagrams. As shown in Fig. 7, especially in the middle and lower panels, a significant part of the AGB group forms a clearly separated tail going from the "bluer" part of the diagram into the "redder" part. A small group of post-AGBs tend to be placed in the region of AGB stars, but also seems to remain in its redder part. Multiple stellar systems also tend to occupy a separate region, a significant amount form a tight "cloud" in the "bluer" part of the diagram, which is visible in the middle panel of Fig. 7. However, a group of multiple systems in nonuniform and single objects are spread over the whole diagram.

One of unusual sources in this group of multiple stellar objects corresponds to `BSDL 923 (Dachs LMC 1-11, SSID69)` classified in the SIMBAD database as a cluster. However, elsewhere, this object is classified as a massive star belonging to a young stellar cluster LMC-N30 (Bica *et al.*, 1999; Gouliermis *et al.*, 2003), or as a B supergiant; hence, it is classified as OTHER in a new classification of 197 point sources observed with the Infrared Spectrograph in the SAGE-Spec Legacy program on the Spitzer Space Telescope (Woods *et al.*, 2011). For example, in the diagram S7–L24 vs. N3–L15 (middle panel of Fig. 7) it is the only object classified as a multiple stellar system in the "redder" part of the diagram. Taking into consideration the dense cluster environment of this source, it is possible that our classification is not correct. Thus, unusual objects which are placed in a nonstandard place in the color-color diagrams, tend not to be of a clearly defined type.

As mentioned in Section 2, only 4 objects within the Milky Way Galaxy were found. They occupy a separate region in the "bluer" part of the color-color diagrams. Because of the small number of objects, it is difficult to define any characteristic tendency. Also, background objects tend to occupy separate regions in color-color diagrams, which can especially be seen in Fig. 7. This group forms a "cloud", which is "redder" than the AGB group, but "bluer" than YSOs. Following Ita *et al.* (2008), we can distinguish two main groups of different objects in the diagram S11–L15 vs N3–S11. One is centered around (0.1, 1) and the second around (1.0, 4.0). Ita *et al.* (2008) further separate the first group into sources without circumstellar dust (centered around (0.2, 0.2)) and red giants with circumstellar emission (centered around (0.25, 0.8)). Also, it can be visible in the diagram, as suggested by Ita *et al.* (2008), that red giants become "bluer" and turn red again during their evolution,

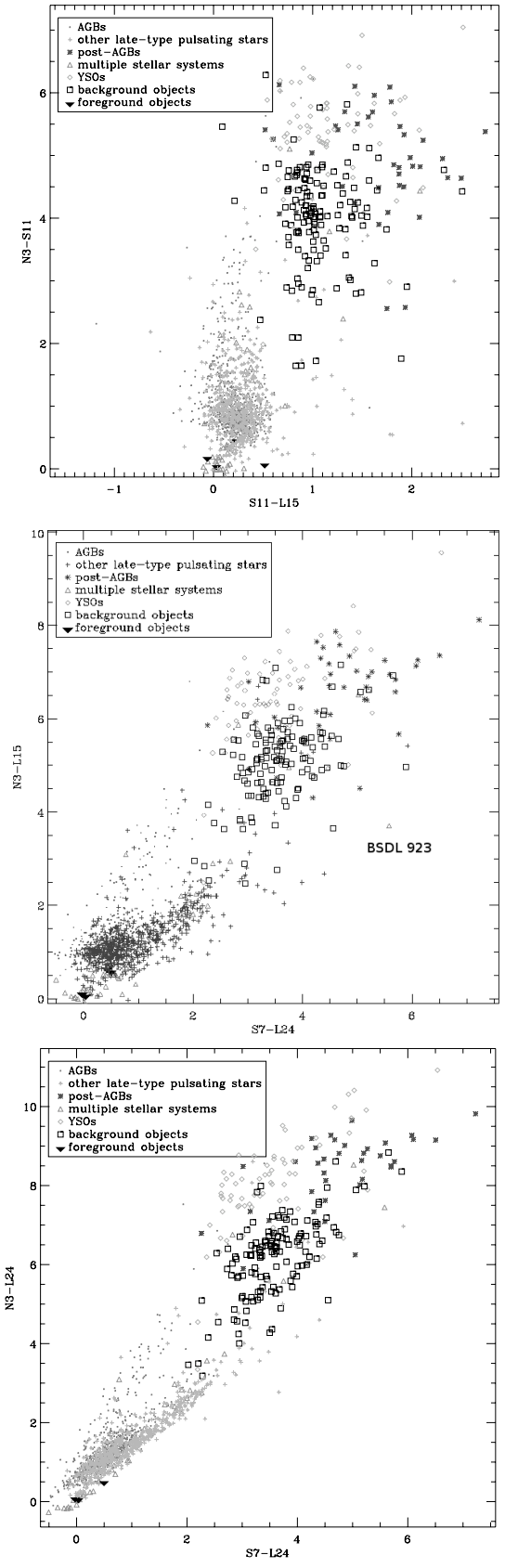

Fig. 7. Position of different types of objects in the color-color diagrams S11–L15 vs. N3–S11 (upper), S7–L24 vs. N3–L15 (middle), S7–L24 vs. N3–L24 (lower). AGB stars are shown as small gray filled circles, other late-type pulsating giants as gray plus signs, post-AGB stars as asterisks, multiple stellar systems as gray open triangles, YSOs as gray diamonds, background objects as black open squares, and foreground objects as black filled triangles.

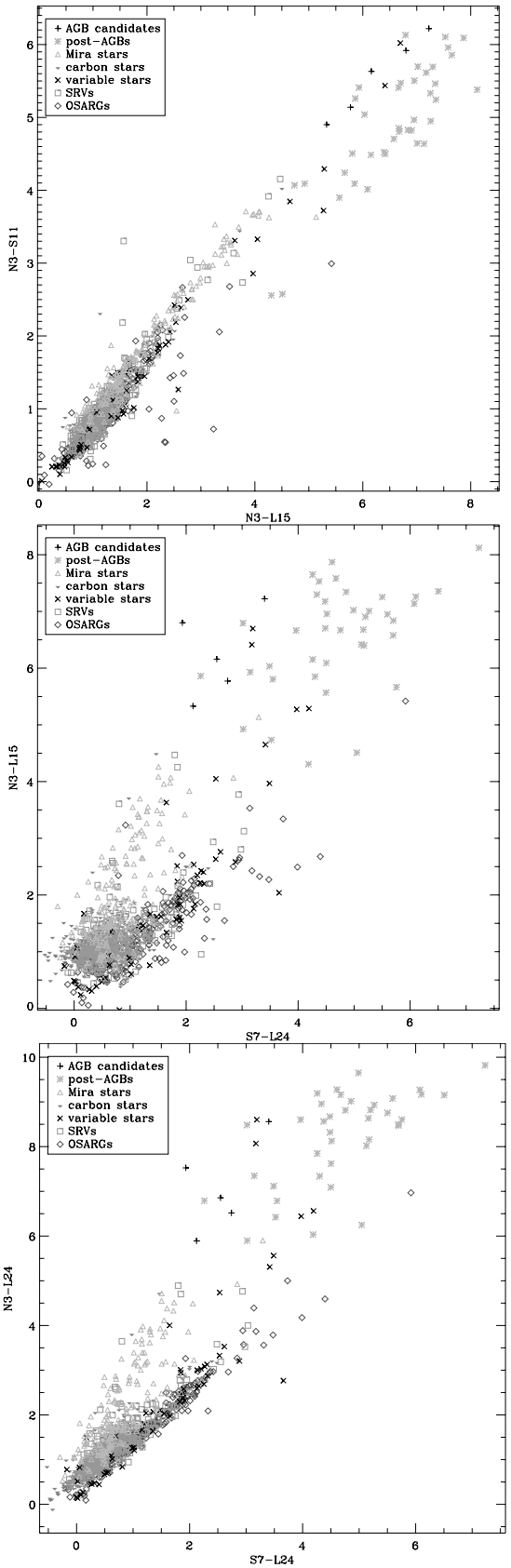

Fig. 8. Position of different types of objects in the color-color diagrams N3–L15 vs. N3–S11 (upper), S7–L24 vs. N3–L15 (middle), S7–L24 vs. N3–L24 (lower). (d) AGB candidates are shown as plus signs, (a) post-AGB stars as gray asterisks, (b) Mira stars as gray open triangles, (c) carbon stars as black filled triangles, (e) variable stars as X signs, (f) SRVs as gray open squares, and (g) OSARGs as diamonds.

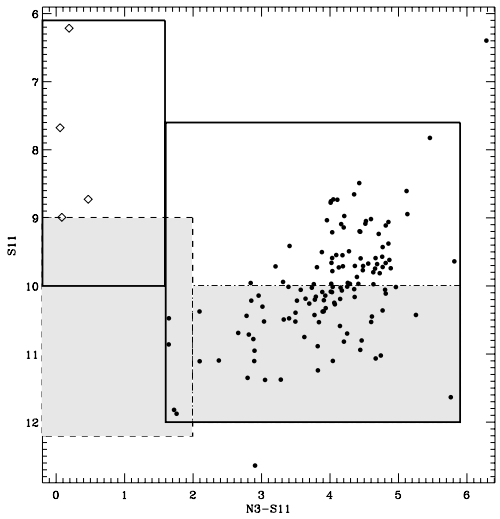

Fig. 9. Color-magnitude diagrams N3–S11 vs S11 (upper) for sources identified as foreground (diamonds) and background objects (filled circles). Objects fulfilling conditions for foreground objects proposed by Ita *et al.* (2008) are placed in the gray area with a dashed outline, objects corresponding to background galaxies have a dash-dotted outline. Modifications of the conditions adapted for our sample is shown with a solid thick outline.

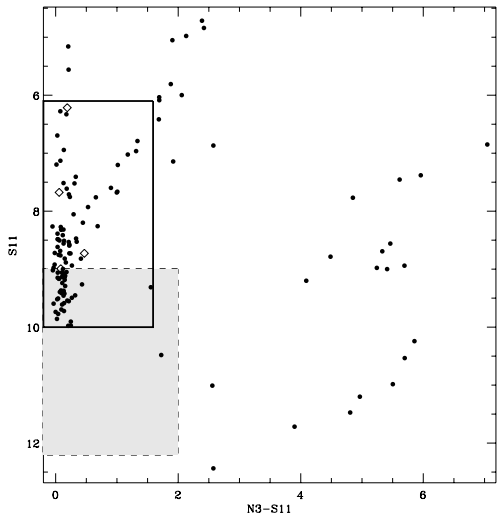

Fig. 10. Color-magnitude diagrams N3–S11 vs S11 for sources suspected of being within Milky Way (filled circles) and classified as foreground objects (diamonds). Objects fulfilling conditions for foreground objects proposed by Ita *et al.* (2008) are placed in gray area with dashed outline, are corresponding for background galaxies have dash-doted outline. Modifications of conditions adapted for our sample is shown with solid thick outline.

which may be caused by changes of strength of silicate, or silicon carbide, dust features in the S11 band relative to the L15 band (Ita *et al.*, 2008). Ita *et al.* (2008) separate a large group of YSO candidates, including PPNe and PNe, which satisfies the condition (N3–S11) $>$ 2.0 and (S11–L15) $>$ 1.0. Also, background galaxies fulfill this restriction (Ita *et al.*, 2008). This condition also restricts our group to YSOs and background objects. Moreover, we can separate a group of YSOs (contaminated by some PNe) in the diagram S11–L15 vs N3–S11, shown in the upper panel of Fig. 7, by the following conditions:

- N3–S11 $>$ 4.5,
- S11–L15 $>$ 0.5.

4.2 Separation of AGB and Post-AGB Stars in Color-Color Diagrams

Color-color diagrams with near- and mid-infrared wavelengths are a useful tool for discriminating various types of AGB, and post-AGB, stars. In the next step, we analyze AGB, and post-AGB, stars from our sample selecting, as in Section 3.2, the following types: (a) post-AGB stars (PNs), (b) Mira stars, (c) carbon stars, (d) candidates for AGB stars, (e) variable stars, (f) semiregular variables (SRV), (g) OGLE small amplitude red giants (OSARG). Color-color diagrams with different types of AGB, and post-AGB, stars are presented in Fig. 8. In all diagrams, carbon stars form a clear cloud in the "bluer" parts of the diagram. Also, post-AGBs, which occupy the "redder" part, are well separated. Mira variables create a long tail going from carbon stars, and become "redder". Candidates for AGBs form a cloud around carbon stars. However, AGB stars appear in a cloud of carbon stars while candidates for AGBs tend to form an adjacent group to carbon stars, but a little bit "bluer".

5. Background Objects and Foreground Milky Way Sources

We distinguish a group of foreground and background objects in our sample during the analysis. Stars denoted as objects within the Milky Way Galaxy in the NED database were classified as foreground objects. We have found only 4 sources fulfilling this criterion, although we expected to find more. As background objects, we selected 133 objects classified as a galaxy or QSO or AGN. As shown in the color-magnitude diagrams N3–S11 vs S11 with identified foreground and background objects, presented in Fig. 9, not all sources fulfill the conditions proposed by Ita *et al.* (2008). Our sample of background objects includes not only galaxies but also AGNs and QSOs, but it is a small group. Taking into consideration the small amount of foreground objects, it is difficult to propose any separation. Based on diagram N3–S11 vs. S11 for our sample, following modifications of these conditions, the following can be proposed:

1) Background objects:

   - N3–S11 $>$ 1.6 [mag],
   - 7.6 $<$ S11 [mag] $<$ 12 .

2) Foreground objects;

   - N3–S11 $<$ 1.6 [mag],
   - 6.1 $<$ S11 [mag] $<$ 10.

However, Ita *et al.* (2008) expected to detect about 500 background galaxies and 190 foreground objects in a square degree and the fraction of foreground stars was estimated to be about 13%. In our sample, less than 0.1% are foreground objects. Thus, we searched for candidates for Galactic objects taking into consideration sources with $z < 0.000927$[2]. This condition was met by 132 objects, mostly classified as other (60%). Among these, 47 sources satisfied the con-

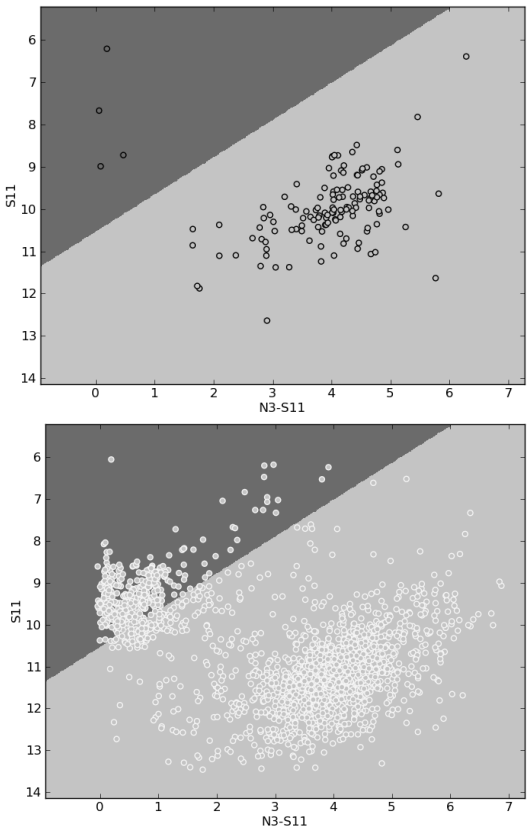

Fig. 11. Color-magnitude diagram N3–S11 vs S11 for sources identified as background, or foreground, objects (upper), and not identified (lower) with the classification based on SVM. The dark gray area is corresponds to sources within the Milky Way, and the light gray area to background objects.

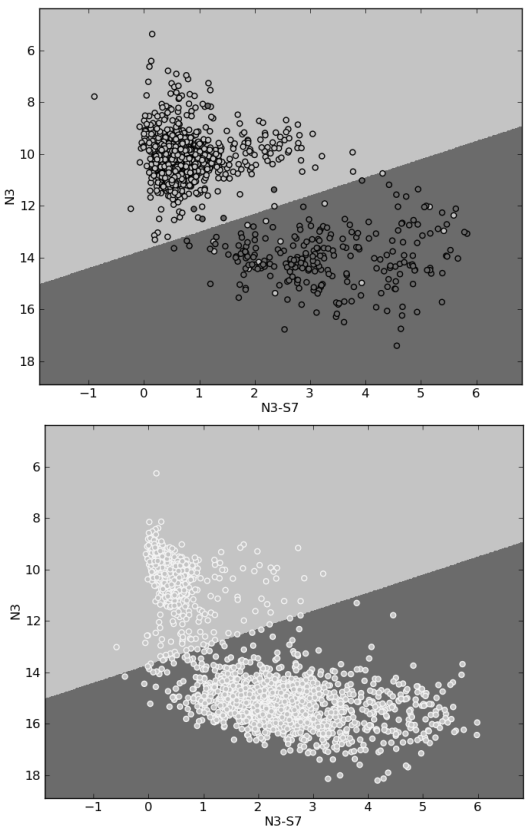

Fig. 12. Color-magnitude diagram N3–S7 vs N3 for sources identified as (1) foreground objects, AGBs, possible AGB, stars and multiple stars (light gray area), or (2) post-AGBs, YSOs and background objects (dark gray area) (upper panel) and not identified (lower panel) with classification based on SVM. Dark gray area is corresponding to objects classified as foreground objects, AGBs, possible AGB stars, or multiple stars. The light gray area corresponds to post-AGBs, YSOs, and background objects.

ditions proposed by Ita *et al*. (2008), and this became 113 objects after taking into consideration our modifications.

6. Sources without Counterparts

For our analysis, we have selected 3 852 sources with complete five-band color information. However, for almost a quarter of them, no counterparts in the NED, SIMBAD, OGLE, 2MASS or AKARI-FIS databases were found (1 016). Moreover, for 872 sources with identified counterparts, a type of object was not determined. In this section, we present further analysis of these sources (1 888) and we discuss the color-magnitude and color-color diagrams. In order to determine the possible types and properties of these sources, we estimate standard fields of different objects at infrared diagrams and discuss the alignment of sources not identified.

To assign different types of sources to different areas of diagrams, we used the classification algorithm from Scikit-learn (Pedregosa *et al*., 2011) based on a Support Vector Machine (SVM) (Chang and Lin, 2011). This is a useful tool used for classification and regression purposes, e.g., to classify structures in the Interstellar Medium (Beaumont *et al*., 2011), or AGNs from stars and normal galaxies (Zhang *et al*., 2002), or to select QSO candidates from the MACHO LMC database (Kim *et al*., 2011a, b).

For our data, a binary classification was performed using a non-linear SVC with a radial basis function (RBF) kernel. The SVM was trained on identified sources. The obtained separation conditions of different group of objects were then used to classify the unknown sources.

6.1 Candidates for foreground and background objects within unidentified sources

Within a sample of unidentified sources, we try to find candidates for background objects and sources within the Milky Way. Our analysis is based on the properties of the diagram N3–S11 vs S11. As a training group to determine separate reference fields, we used sources identified as background, or Galactic, objects. Objects suspected of being foreground or background objects, presented in Section 5, are not taken into consideration.

The color-magnitude diagram N3–S11 vs S11 is presented in Fig. 11. In the upper panel, data used for training are plotted, and in the lower panel unidentified sources are plotted. There is a small amount of identified (upper panel) foreground objects (dark gray area), and a large amount of background objects (light gray area). We found a similar tendency in the case of the unidentified sources. A dominant number of sources without counterparts are placed in

[2]Information about the values of z is taken from the SIMBAD database.

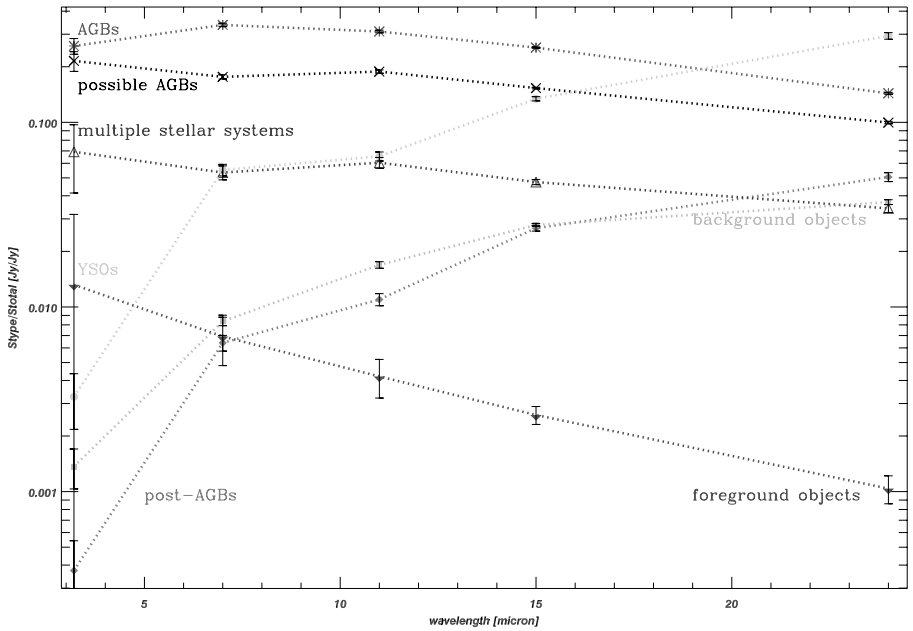

Fig. 13. Contribution of different types of objects to the total number of point sources detected in NIR and MIR at each band ($S_{\rm total}$). AGB stars are shown as asterisks, late-type pulsating giants as X sign, multiple stellar systems as triangles, YSOs as diamonds, post-AGB as filled diamonds, background objects as squares, foreground objects as filled triangles, other as circles, sources of an unknown origin as filled squares, and sources not identified as filled circles.

the light gray area, corresponding to background objects.

6.2 Separation of sources without counterparts in color-magnitude diagrams

As shown in Section 3, based on color-magnitude diagrams, we can see separation between different types of objects. We tried to classify not identified sources using a diagram N3–S7 vs S7. In Fig. 5 (upper panel), we can see a clear separation between two clouds: one formed by foreground objects, AGBs, and possible AGB stars, and multiple stellar systems; and a second one consisting of post-AGBs, YSOs, and background sources. We used these two groups to train the SVM and the result is presented in the upper panel of Fig. 12. Within a sample the "bluer", and more luminous, group is significantly larger than the "redder" one (1 409: 243). Taking into consideration sources not identified, this dependence is opposite, i.e., more sources tend to be post-AGBs, YSOs, or background objects.

7. Contribution from Main Sources to the Total Infrared Flux in the LMC

Observations made using the Spitzer Space Telescope have enabled gas and dust input from AGB stars to be studied in the LMC (Matsuura *et al.*, 2009). The dominant source of gas are AGBs and possibly supernovea; however, present-day star formation depends on gas already present in the ISM. Thus, the star-formation rate will probably decline, when gas in the ISM becomes exhausted, unless another gas feedback is provided (Matsuura *et al.*, 2009). Matsuura *et al.* (2009) suggest that the LMC have common for high-z galaxies 'a missing dust-mass problem'. Dust mass contributed from AGBs and SNe over the dust life time is significantly less than the dust mass in the ISM, so another source of dust is required (Matsuura *et al.*, 2009). AGBs, especially those carbon-rich, are a dominant source of gas and dust for the ISM of the LMC. Dust production from SNe is very uncertain; however, SNe are important contributors of gas. Also, novae and R CrB stars can expel dust and gas to the ISM, however their feedback is minor (Matsuura *et al.*, 2009).

The contribution from different objects to the total NIR and MIR flux is shown in Fig. 13. In all the NIR and MIR wavelengths, AGB stars are the dominant source of LMC radiation from point sources, which corresponds to their number percent. YSOs, and post-AGBs, are more visible at longer wavelengths, while AGBs contribute more and more when we move to shorter wavelengths. Objects with an unknown origin also, as post-AGBs and YSOs, contribute more at longer wavelengths. The luminosity contribution of foreground objects falls mainly within the wavelength range 3 to 24 μm, contrary to the contribution from background objects.

8. Summary

The AKARI IRC survey performed observations over an area of about 10 deg^2 of the Large Magellanic Cloud. We prepared a catalog of counterparts based on the Release Candidate version 1 of the point source catalog of the AKARI LMC Large Area Survey. Our analysis is based on sources detected at all NIR and MIR wavelengths of 3.2, 7.0, 11.0, 15.0, 24.0 μm, i.e. with a complete five-band color information. We cross-correlated these sources with publicly-available databases at different wavelengths and found counterparts for almost 75% of our sample. A majority (nearly 70%) of identified sources are AGB stars and similar evolved giants. Consequently, AGB stars are the dominant source of the LMC radiation at all NIR and MIR wavelengths from point sources. Their luminosity contribu-

tion rises with wavelength from 3 to 24 μm, contrary to the contribution from YSOs and PNe. This IR budget should be useful for future modeling of detailed SEDs of LMC-like irregular galaxies. In this paper, we have also presented color-magnitude, and color-color, diagrams showing new interesting features. We have distinguished different groups of AGBs, and post-AGBs, and discussed color-magnitude, and color-color, diagrams. Within a sample there is a large number of sources without counterparts, or of an unidentified type, for which we present color-magnitude diagrams. Using an SVM, we have proposed a method to determine the properties of unidentified objects from their infrared color information.

Acknowledgments. We thank both referees for providing constructive comments and help in improving this paper. This work is based on observations with AKARI, a JAXA project with the participation of ESA. This research has made use of the NASA/IPAC Extragalactic Database (NED) which is operated by the Jet Propulsion Laboratory, California Institute of Technology, under contract with the National Aeronautics and Space Administration, and the SIMBAD database, operated at CDS, Strasbourg, France. AP and MS have been supported by the research grant of the Polish Ministry of Science N N203 51 29 38. This research was partially supported by the project POLISH-SWISS ASTRO PROJECT co-financed by a grant from Switzerland through the Swiss Contribution to the enlarged European Union. TTT has been supported by the Grant-in-Aid for the Scientific Research Fund (20740105, 23340046, and 24111707) and for the Global COE Program Request for Fundamental Principles in the Universe: from Particles to the Solar System and the Cosmos commissioned by the Ministry of Education, Culture, Sports, Science and Technology (MEXT) of Japan.

References

Alves, D. R., A review of the distance and structure of the Large Magellanic Cloud, *New Astron. Rev.*, **48**, 659–665, 2004.

Asano, R. S., T. T. Takeuchi, H. Hirashita, and A. K. Inoue, Dust formation history of galaxies: A critical role of metallicity for the dust mass growth by accreting materials in the interstellar medium, *Earth Planets Space*, **65**, this issue, 213–222, 2013.

Beaumont, C. N., J. P. Williams, and A. A. Goodman, Classifying structures in the ISM with Support Vector Machines: the G16.05-0.57 supernova remnant, *ArXiv e-prints*, arXiv:1107.5584, 2011.

Bica, E. L. D., H. R. Schmitt, C. M. Dutra, and H. L. Oliveira, A revised and extended catalog of Magellanic system clusters, associations, and emission nebulae. II. The Large Magellanic Cloud, *Astron. J.*, **117**, 238–246, 1999.

Blum, R. D. *et al.*, Spitzer SAGE survey of the Large Magellanic Cloud. II. Evolved stars and infrared color-magnitude diagrams, *Astron. J.*, **132**, 2034–2045, 2006.

Bonanos, A. Z. *et al.*, Spitzer SAGE infrared photometry of massive stars in the Large Magellanic Cloud, *Astron. J.*, **138**, 1003–1021, 2009.

Chang, C. C. and C. J. Lin, LIBSVM: A library for support vector machines, *ACM Trans. Intell. Syst. Technol.*, **2**, 27:1–27:27, 2011.

Cutri, R. M. *et al.*, 2MASS All Sky Catalog of point sources, *The IRSA 2MASS All-Sky Point Source Catalog, NASA/IPAC Infrared Science Archive*, 2003.

Davies, R. D., K. H. Elliott, and J. Meaburn, The nebular complexes of the large and small Magellanic Clouds, *Mem. R. Astron. Soc.*, **81**, 89–128, 1976.

de Vaucouleurs, G. and K. C. Freeman, Structure and dynamics of barred spiral galaxies, in particular of the Magellanic type, *Vistas Astron.*, **14**, 163–294, 1972.

Egan, M. P., S. D. Price, and K. E. Kraemer, The Midcourse Space Experiment Point Source Catalog Version 2.3, *Bull. Am. Astron. Soc.*, **35**, 1301, 2003.

Fazio, G. G. *et al.*, The Infrared Array Camera (IRAC) for the Spitzer Space Telescope, *Astrophys. J. Suppl. Ser.*, **154**, 10, 2004.

Fukui, Y., Giant molecular clouds in the Magellanic Clouds, *The Cool Universe: Observing Cosmic Dawn*, **344**, 155, 2005.

Fukui, Y. *et al.*, The second survey of the molecular clouds in the Large Magellanic Cloud by NANTEN. I. Catalog of Molecular Clouds, *Astrophys. J. Suppl. Ser.*, **178**, 56–70, 2008.

Gallagher, J. S., III and D. A. Hunter, Structure and evolution of irregular galaxies, *Ann. Rev. Astron. Astrophys.*, **22**, 37–74, 1984.

Gouliermis, D., M. Kontizas, E. Kontizas, and R. Korakitis, OB stellar associations in the Large Magellanic Cloud: Survey of young stellar systems, *Astron. Astrophys.*, **405**, 111–124, 2003.

Groenewegen, M. A. T. *et al.*, Luminosities and mass-loss rates of carbon stars in the Magellanic Clouds, *Mon. Not. R. Astron. Soc.*, **376**, 313–337, 2007.

Henize, K. G., Catalogues of Hα-EMISSION stars and nebulae in the Magellanic Clouds, *Astrophys. J. Suppl. Ser.*, **2**, 315, 1956.

Hora, J. L. *et al.*, Spitzer sage observations of Large Magellanic Cloud planetary nebulae, *Astron. J.*, **135**, 726–736, 2008.

Hunter, D., Star formation in irregular galaxies: A review of several key questions, *Publ. Astron. Soc. Pac.*, **109**, 937–950, 1997.

Hunter, D. A., Star-forming regions in irregular galaxies (review), *Modes of Star Formation and the Origin of Field Populations*, **285**, 323, 2002.

Hunter, D. A. and J. S. Gallagher, III, Stellar populations and star formation in irregular galaxies, *Publ. Astron. Soc. Pac.*, **98**, 5–28, 1986.

Hunter, D. A. and Elmegreen B. G., Star formation properties of a large sample of irregular galaxies, *Astron. J.*, **128**, 2170–2205, 2004.

Ishihara, D. *et al.*, Mid-infrared All-Sky Survey with the Infrared Camera (IRC) on board the ASTRO-F satellite, *Publ. Astron. Soc. Pac.*, **118**, 324–343, 2006.

Ita, Y. *et al.*, AKARI IRC Survey of the Large Magellanic Cloud: Outline of the survey and initial results, *Publ. Astron. Soc. Jpn.*, **60**, 435, 2008.

Ita, Y., T. Onaka, and D. Kato, AKARI IRC survey of the Large Magellanic Cloud: A new feature in the infrared color-magnitude diagram, *IAU Symposium*, **256**, 9–13, 2009.

Karachentseva, V. E., S. N. Mitronova, O. V. Melnyk, and I. D. Karachentsev, Catalog of isolated galaxies selected from the 2MASS survey, *Astrophys. Bull.*, **65**, 1–17, 2010.

Kato, D., T. Onaka, and Y. Ita, Akari LMC Team, AKARI IRC Survey of the Large Magellanic Cloud, *AKARI, a Light to Illuminate the Misty Universe*, **418**, 149, 2009.

Kato, D. *et al.*, The IRSF Magellanic Clouds Point Source Catalog, *Publ. Astron. Soc. Jpn.*, **59**, 615–641, 2007.

Kato *et al.*, in prep.

Kawada, M. *et al.*, The Far-Infrared Surveyor (FIS) for AKARI, *Publ. Astron. Soc. Jpn.*, **59**, 389, 2007.

Kim, D.-W., P. Protopapas, C. Alcock, Y. Byun, and R. Khardon, Automatic QSO selection algorithm using time series analysis and machine learning, *Bull. Am. Astron. Soc.*, **43**, #116.01, 2011a.

Kim, D.-W., P. Protopapas, Y.-I. Byun, C. Alcock, R. Khardon, and M. Trichas, Quasi-stellar object selection algorithm using time variability and machine learning: Selection of 1620 quasi-stellar object candidates from MACHO Large Magellanic Cloud database, *Astrophys. J.*, **735**, 68, 2011b.

Koornneef, J., The gas to dust ratio and the near-infrared extinction law in the Large Magellanic Cloud, *Astron. Astrophys.*, **107**, 247–251, 1982.

Longair, M. S., Galaxy formation, in *Galaxy Formation*, Springer, Berlin, 2008.

Luck, R. E., T. J. Moffett, T. G. Barnes, III, and W. P. Gieren, Magellanic Cloud Cepheids—Abundances, *Astron. J.*, **115**, 605, 1998.

Manteiga, M., D. A. García-Hernández, A. Ulla, A. Manchado, and P. García-Lario, IRAS 17423-1755 (Hen 3-1475) revisited: An O-rich high-mass post-asymptotic giant branch star, *Astron. J.*, **141**, 80, 2011.

Matsuura, M. *et al.*, The global gas and dust budget of the Large Magellanic Cloud: AGB stars and supernovae, and the impact on the ISM evolution, *Mon. Not. R. Astron. Soc.*, **396**, 918–934, 2009.

Meixner, M. *et al.*, Spitzer Survey of the Large Magellanic Cloud: Surveying the Agents of a Galaxy's Evolution (SAGE). I. Overview and initial results, *Astron. J.*, **132**, 2268–2288, 2006.

Meixner, M. *et al.*, HERschel Inventory of The Agents of Galaxy Evolution (HERITAGE): The Large Magellanic Cloud dust, *Astron. Astrophys.*, **518**, L71–, 2010.

Murakami, H. *et al.*, The infrared astronomical mission AKARI, *Publ. Astron. Soc. Jpn.*, **59**, 369, 2007.

Nota, A. *et al.*, Discovery of a population of pre-main-sequence stars in NGC 346 from deep Hubble Space Telescope ACS images, *Astrophys. J.*, **640**, L29–L33, 2006.

Onaka, T. *et al.*, The Infrared Camera (IRC) for AKARI—Design and imaging performance, *Publ. Astron. Soc. Jpn.*, **59**, 401, 2007.

Onaka, T. *et al.*, AKARI large area survey of the Large Magellanic Cloud, *The Evolving ISM in the Milky Way and Nearby Galaxies*, 2009.

Pedregosa, F. *et al.*, Scikit-learn: Machine learning in Python, *J. Mac. Learn. Res.*, **12**, 2825–2830, 2011.

Poleski, R. *et al.*, The optical gravitational lensing experiment. The OGLE-III catalog of variable stars. VI. Delta Scuti stars in the Large Magellanic Cloud, *Acta Astron.*, **60**, 1–16, 2010a.

Poleski, R., I. Soszyński, A. Udalski, M. K. Szymański, M. Kubiak, G. Pietrzyński, Ł. Wyrzykowski, and K. Ulaczyk, The optical gravitational lensing experiment. The OGLE-III catalog of variable stars. X. enigmatic class of double periodic variables in the Large Magellanic Cloud, *Acta Astron.*, **60**, 179–196, 2010b.

Sakon, I., T. Onaka, H. Kaneda, D. Tokura, T. Takagi, Y. Y. Tajiri, H. Takahashi, D. Kato, T. Onishi, A. Kawamura, and Y. Fukui, The properties of the mid- to far-infrared emission in the Large Magellanic Cloud, *Astrophys. J.*, **651**, 174–189, 2006.

Shimonishi, T., T. Onaka, D. Kato, I. Sakon, Y. Ita, A. Kawamura, and H. Kaneda, Spectroscopic observations of ices around embedded young stellar objects in the Large Magellanic Cloud with AKARI, *Astron. Astrophys.*, **514**, A12, 2010.

Skrutskie, M. F. *et al.*, The 2MASS extended sources (IPAC/UMass, 2003-2006), *VizieR Online Data Catalog*, **7233**, 0, 2003.

Skrutskie, M. F. *et al.*, The Two Micron All Sky Survey (2MASS), *Astron. J.*, **131**, 1163–1183, 2006.

Soszyński, I. *et al.*, The optical gravitational lensing experiment. The OGLE-III catalog of variable stars. II. type II Cepheids and anomalous Cepheids in the Large Magellanic Cloud, *Acta Astron.*, **58**, 293, 2008a.

Soszyński, I. *et al.*, The optical gravitational lensing experiment. The OGLE-III catalog of variable stars. I. Classical Cepheids in the Large Magellanic Cloud, *Acta Astron.*, **58**, 163–185, 2008b.

Soszyński, I. *et al.*, The optical gravitational lensing experiment. The OGLE-III catalog of variable stars. V. R Coronae Borealis stars in the Large Magellanic Cloud, *Acta Astron.*, **59**, 335–347, 2009a.

Soszyński, I. *et al.*, The optical gravitational lensing experiment. The OGLE-III catalog of variable stars. III. RR Lyrae stars in the Large Magellanic Cloud, *Acta Astron.*, **59**, 1–18, 2009b.

Soszyński, I. *et al.*, The optical gravitational lensing experiment. The OGLE-III catalog of variable stars. IV. Long-period variables in the Large Magellanic Cloud, *Acta Astron.*, **59**, 239–253, 2009c.

Srinivasan, S. *et al.*, The mass loss return from evolved stars to the Large Magellanic Cloud: Empirical relations for excess emission at 8 and 24 μm, *Astron. J.*, **137**, 4810–4823, 2009.

Tanabé, T. *et al.*, Absolute photometric calibration of the Infrared Camera (IRC) aboard AKARI, *Publ. Astron. Soc. Jpn.*, **60**, 375, 2008.

van Aarle, E., H. van Winckel, T. L. Evans, and P. R. Wood, The optically bright post-AGB population of the LMC, *IAU Symposium*, **256**, 415–420, 2009.

van der Marel, R. P. and M.-R. L. Cioni, Magellanic Cloud structure from near-infrared surveys. I. The viewing angles of the Large Magellanic Cloud, *Astron. J.*, **122**, 1807–1826, 2001.

van Loon, J. T., A. A. Zijlstra, and M. A. T. Groenewegen, Luminous carbon stars in the Magellanic Clouds, *Astron. Astrophys.*, **346**, 805–810, 1999.

van Loon, J. T. *et al.*, A Spitzer Space Telescope far-infrared spectral atlas of compact sources in the Magellanic Clouds. I. The large Magellanic Cloud, *Astron. J.*, **139**, 68–95, 2010.

Vijh, U. P. *et al.*, Variable evolved stars and young stellar objects discovered in the Large Magellanic Cloud using the SAGE survey, *Astron. J.*, **137**, 3139–3148, 2009.

Werner, M. W. *et al.*, The Spitzer Space Telescope Mission, *Astrophys. J. Suppl. Ser.*, **154**, 1–9, 2004.

Whitney, B. A. *et al.*, Spitzer Sage survey of the Large Magellanic Cloud. III. Star formation and ˜1000 new candidate young stellar objects, *Astron. J.*, **136**, 18–43, 2008.

Wilcots, E. M., Magellanic type galaxies throughout the Universe, *IAU Symposium*, **256**, 461–472, 2009.

Woods, P. M. *et al.*, The SAGE-Spec Spitzer Legacy programme: the life-cycle of dust and gas in the Large Magellanic Cloud—Point source classification I, *Mon. Not. R. Astron. Soc.*, **411**, 1597–1627, 2011.

Yamaguchi, R. *et al.*, A CO survey of the LMC with NANTEN: III. Formation of stellar clusters and evolution of molecular clouds, *Publ. Astron. Soc. Jpn.*, **53**, 985–1001, 2001.

Yamamura, I., S. Makiuti, N. Ikeda, Y. Fukuda, S. Oyabu, T. Koga, and G. J. White, AKARI/FIS All-Sky Survey Point Source Catalogues (ISAS/JAXA, 2010), *VizieR Online Data Catalog*, **2298**, 0, 2010.

Zaritsky, D., J. Harris, I. B. Thompson, and E. K. Grebel, The Magellanic Clouds Photometric Survey: The Large Magellanic Cloud Stellar Catalog and Extinction Map, *Astron. J.*, **128**, 1606–1614, 2004.

Zhang, Y., C. Cui, and Y. Zhao, Classification of AGNs from stars and normal galaxies by support vector machines, *Society of Photo-Optical Instrumentation Engineers (SPIE) Conference Series*, **4847**, 371–378, 2002.

M. Siudek (e-mail: gsiudek@cft.edu.pl), A. Pollo, T. T. Takeuchi, Y. Ita, D. Kato, and T. Onaka

Appendix A. Positional Differences for Matched Sources with 2MASS, NED, SIMBAD, AKARI FIS All-Sky Survey, OGLE, Databases

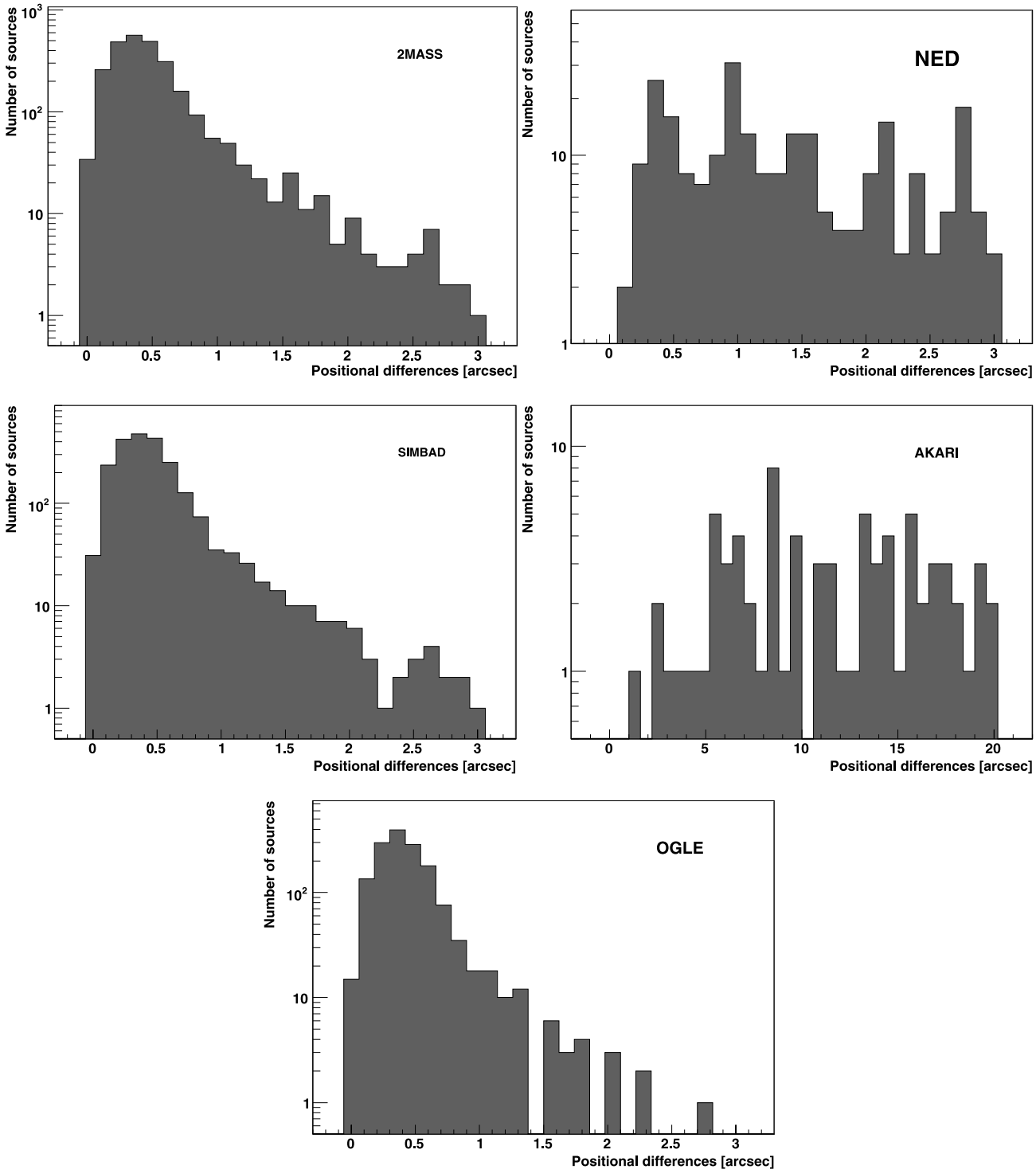

Fig. A.1. The distribution of positional differences between the sources and identified counterparts in 2MASS, NED, SIMBAD, AKARI FIS All-Sky Survey, OGLE. The size of the bin is 0.1 arcsec for the AKARI data, extended to 0.5 arcsec for the FIS data.

Appendix B. Classifiaction of Detected Sources with Complete Color Information

Table B.1. Classification of 1 964 detected sources with complete color information.

LMC objects		1 814	%
	(1) AGB stars	828	42.16
	(2) Other late-type pulsating giants	528	26.88
	(3) Post-AGBs	39	1.99
	(4) Multiple stellar systems	49	2.49
	(5) Young stellar objects	71	3.62
	Other	233	11.86
Sources of unknown origin		79	4.02
(6) Background objects		133	
	Galaxies	126	6.42
	QSO/AGN	7	0.36
(7) Foreground objects		4	0.20

Appendix C. Classification of AGB, Other Late-Type Pulsating Giants, and Post-AGB Stars

Table C.1. Classification of AGB, other late-type pulsating giants, and post-AGB stars.

AGB and post-AGB stars			1 395
	(a) Post-AGB (Planetary Nebulae)		39
	(b) Mira-type stars		181
	(c) Carbon stars		642
	(d) AGB candidates		5
	Other late-type pulsating giants		528
		(e) Variable stars	59
		(f) SRV	303
		(g) OSARG	166

Appendix D. Color-Color Diagrams

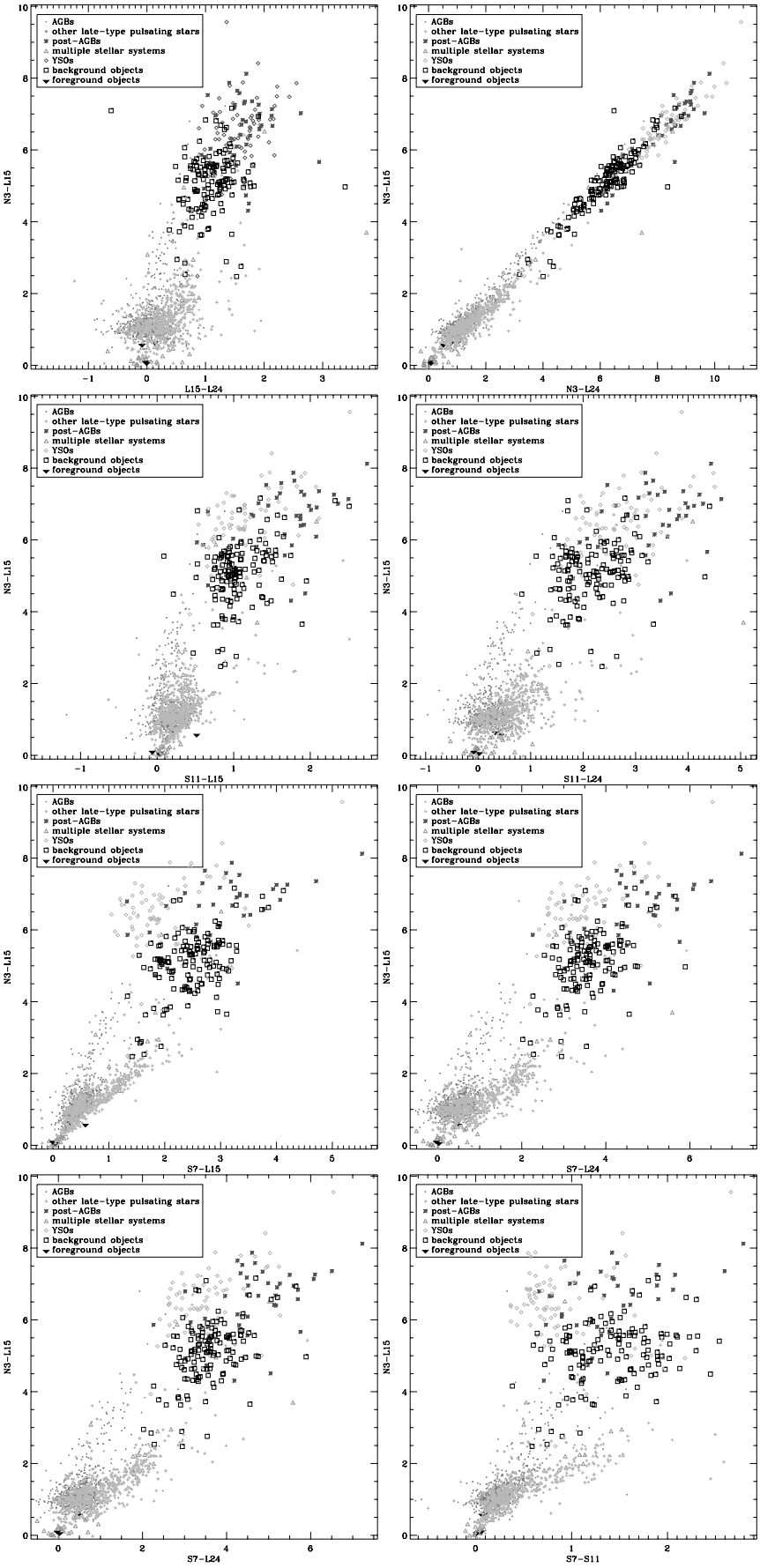

Fig. D.1. Position of different types of objects in the color-color diagrams. All symbols as in Fig. 7.

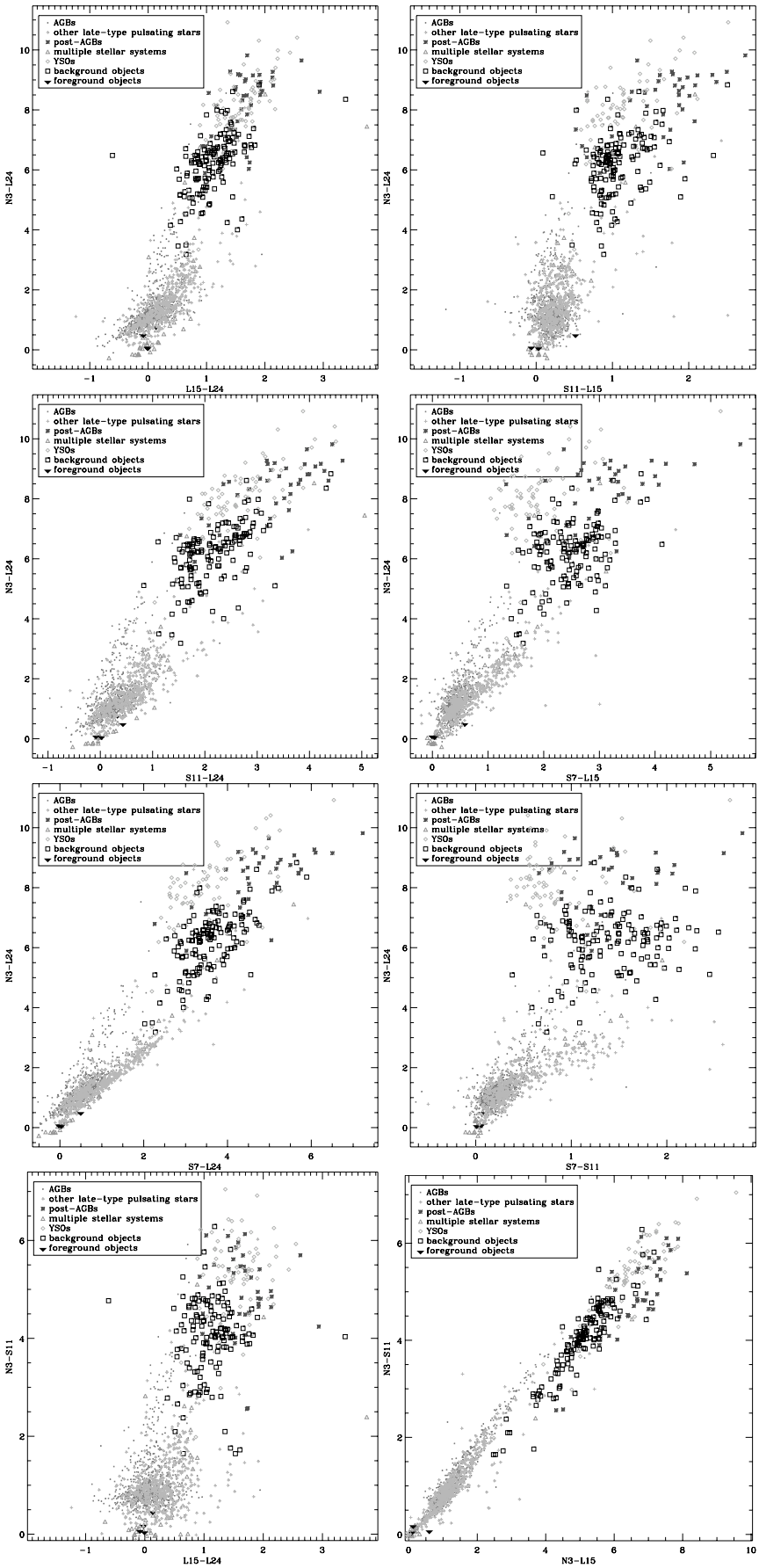

Fig. D.2. Position of different types of objects in the color-color diagrams. All symbols as in Fig. 7.

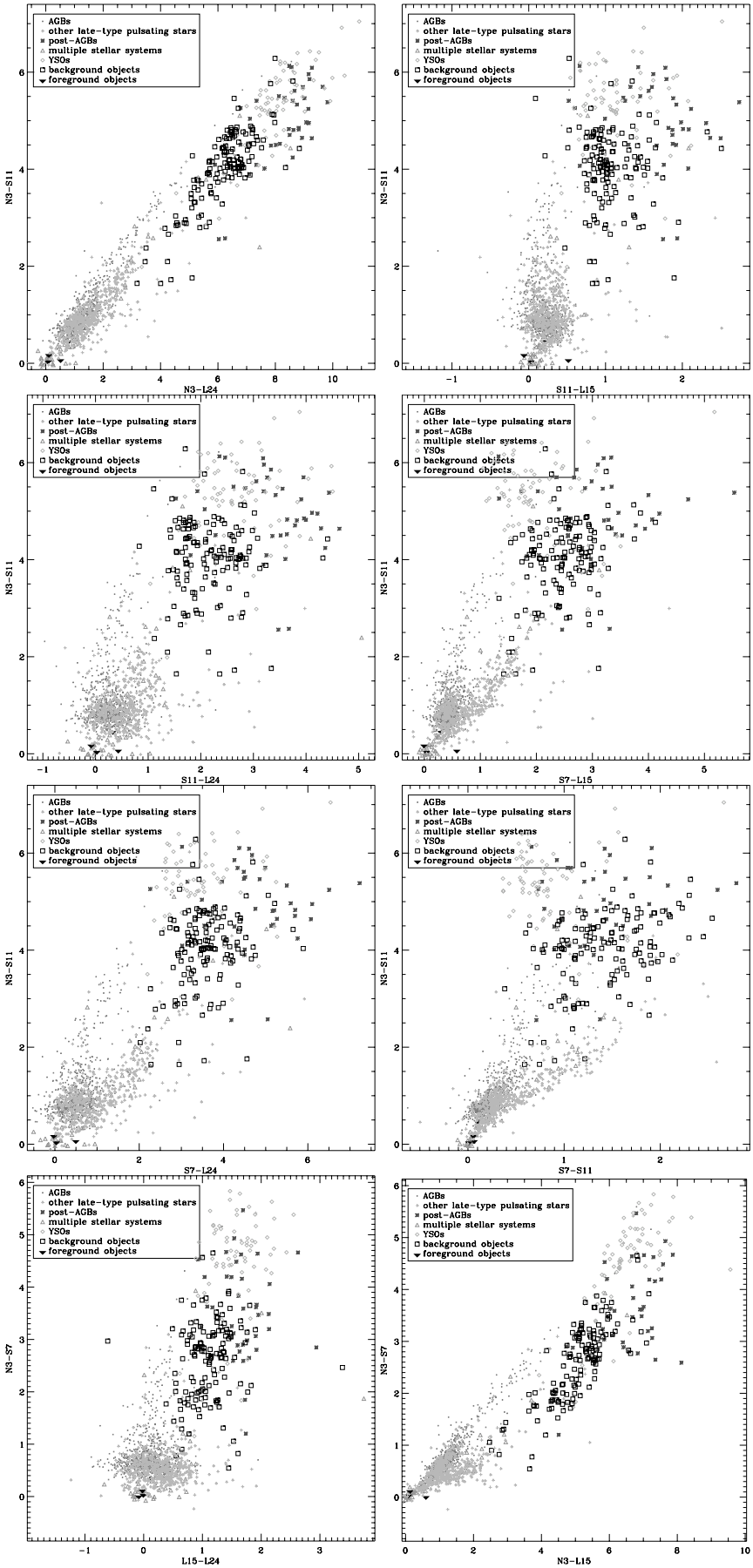

Fig. D.3. Position of different types of objects in the color-color diagrams. All symbols as in Fig. 7.

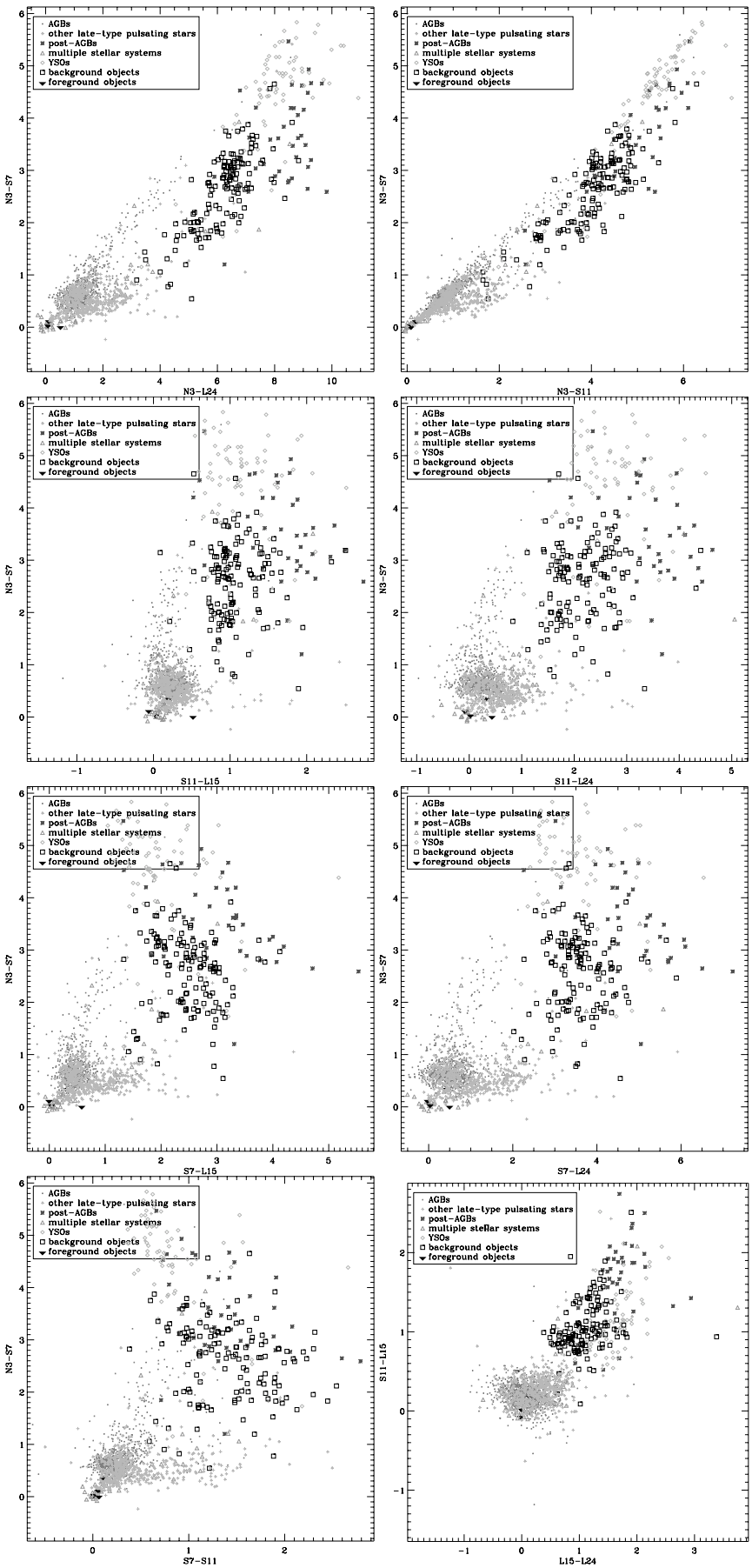

Fig. D.4. Position of different types of objects in the color-color diagrams. All symbols as in Fig. 7.

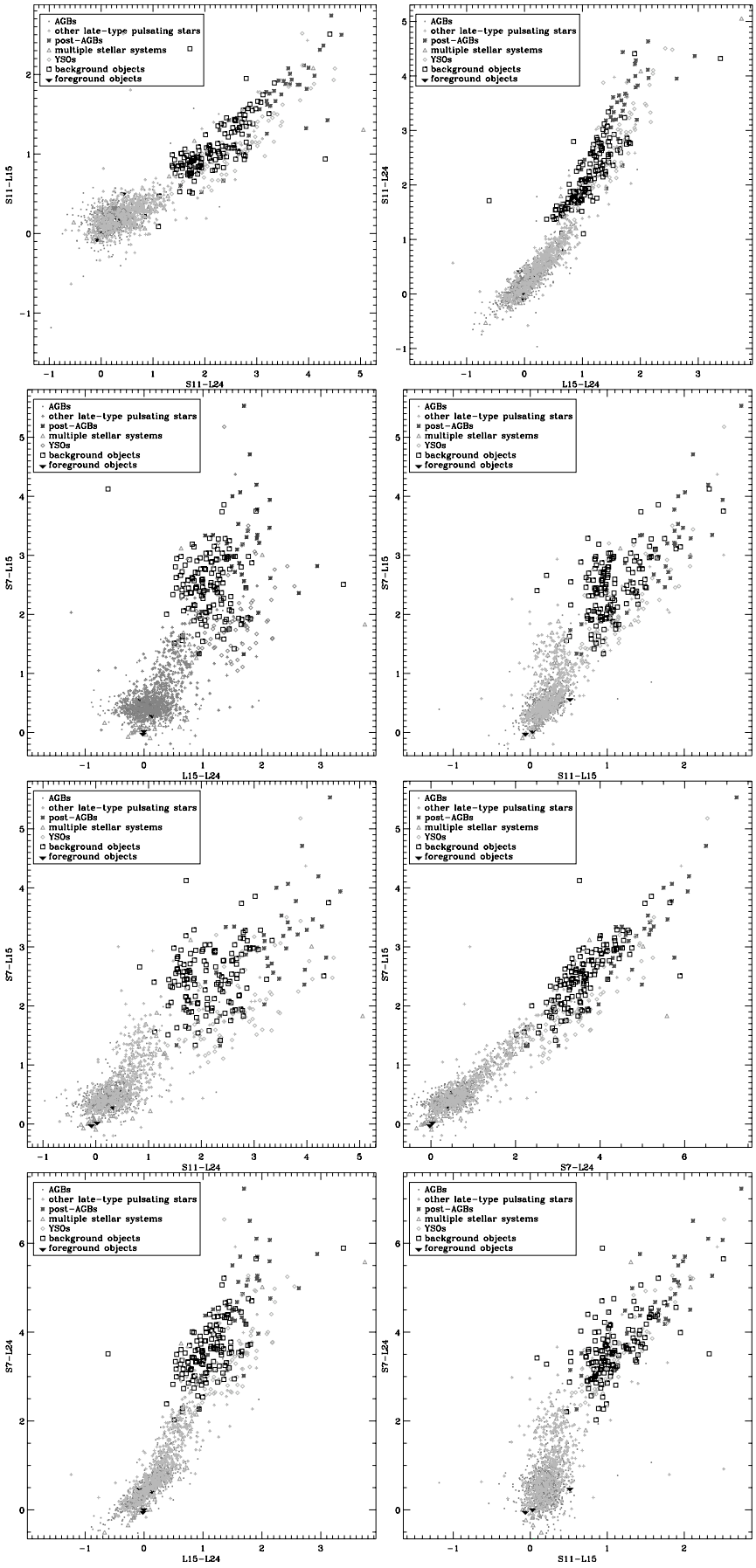

Fig. D.5. Position of different types of objects in the color-color diagrams. All symbols as in Fig. 7.

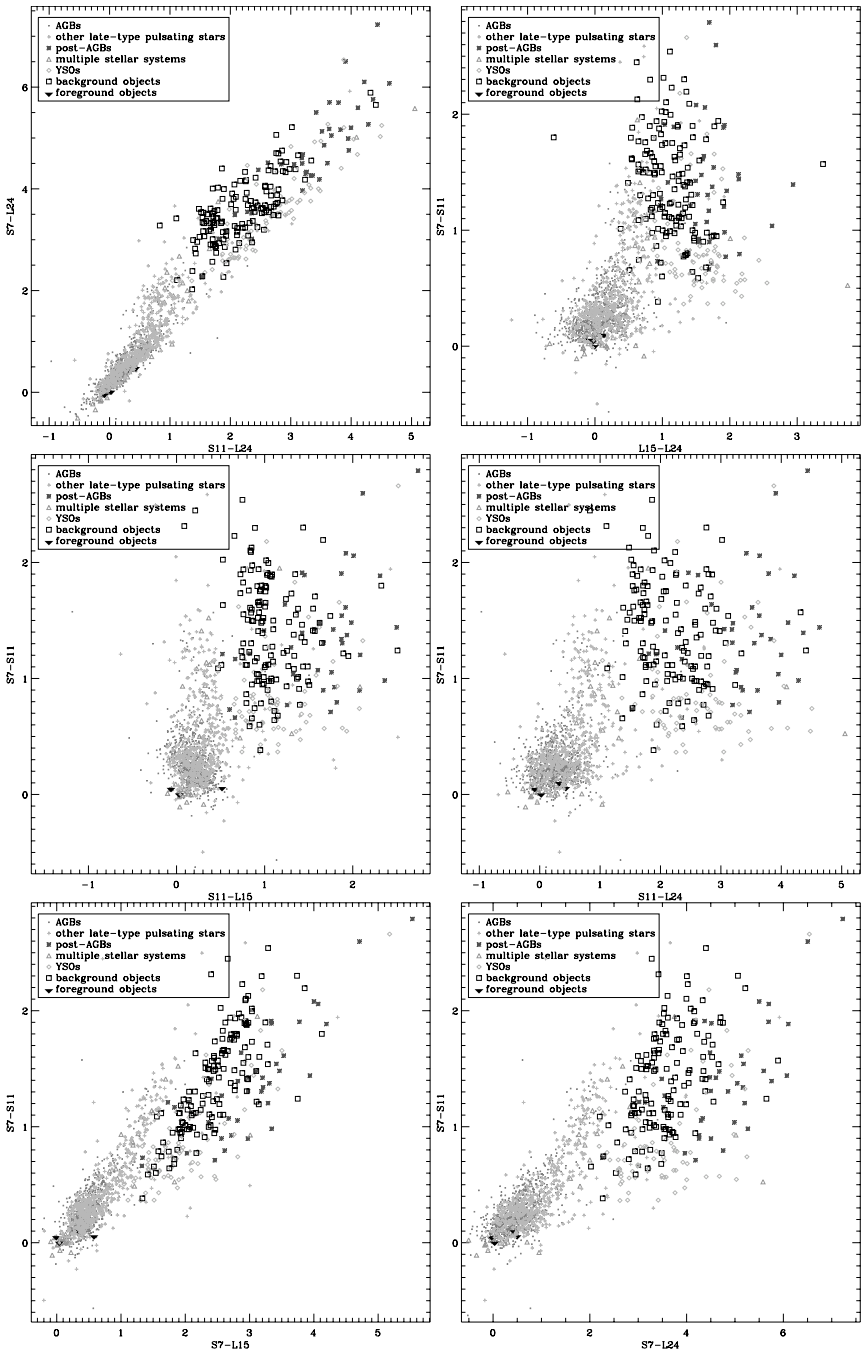

Fig. D.6. Position of different types of objects in the color-color diagrams. All symbols as in Fig. 7.

Appendix E. Color-Color Diagrams

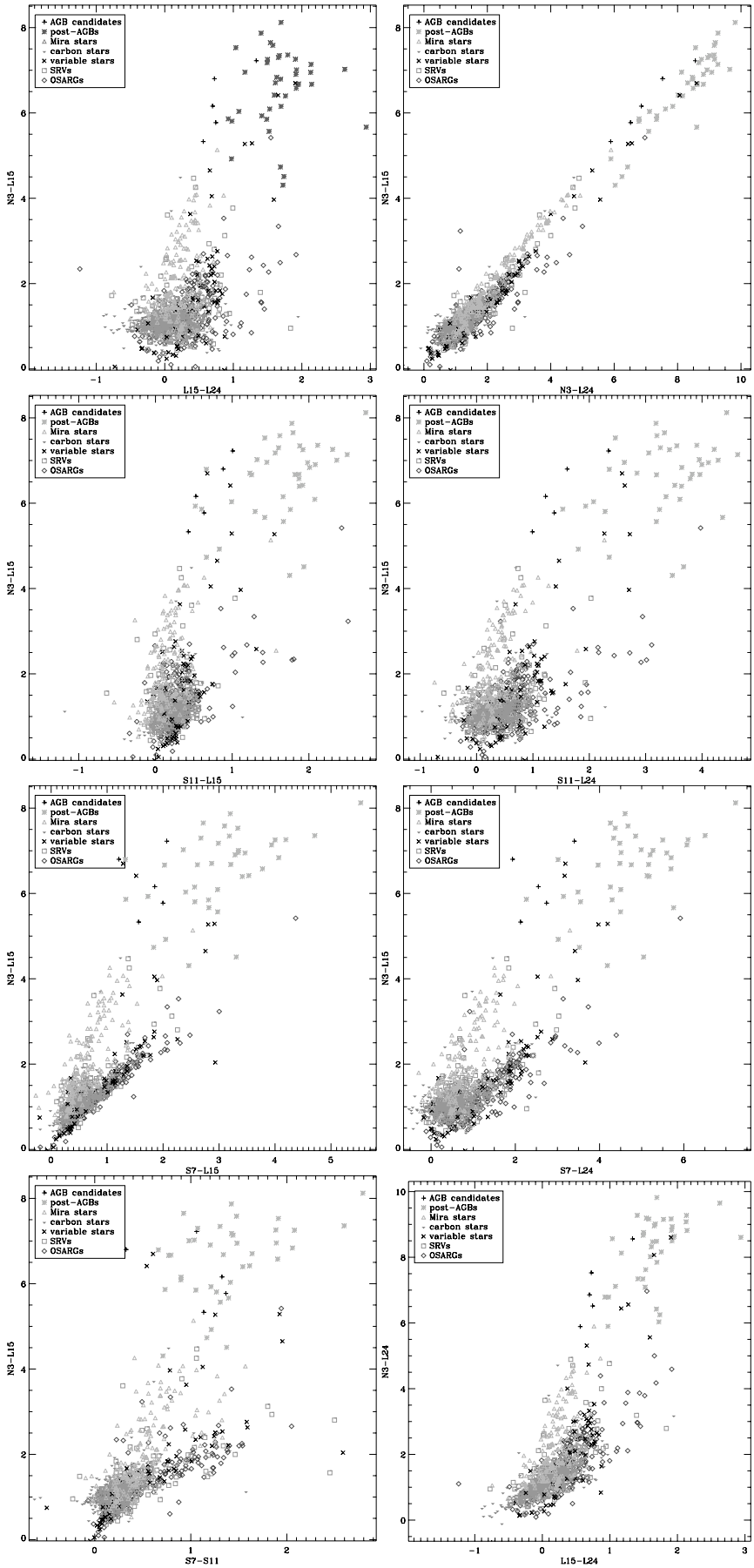

Fig. E.1. Position of AGB stars, late-type pulsating stars, possibly being AGBs or close to the AGB phase, and post-AGB stars in the color-color diagrams. All symbols as in Fig. 8.

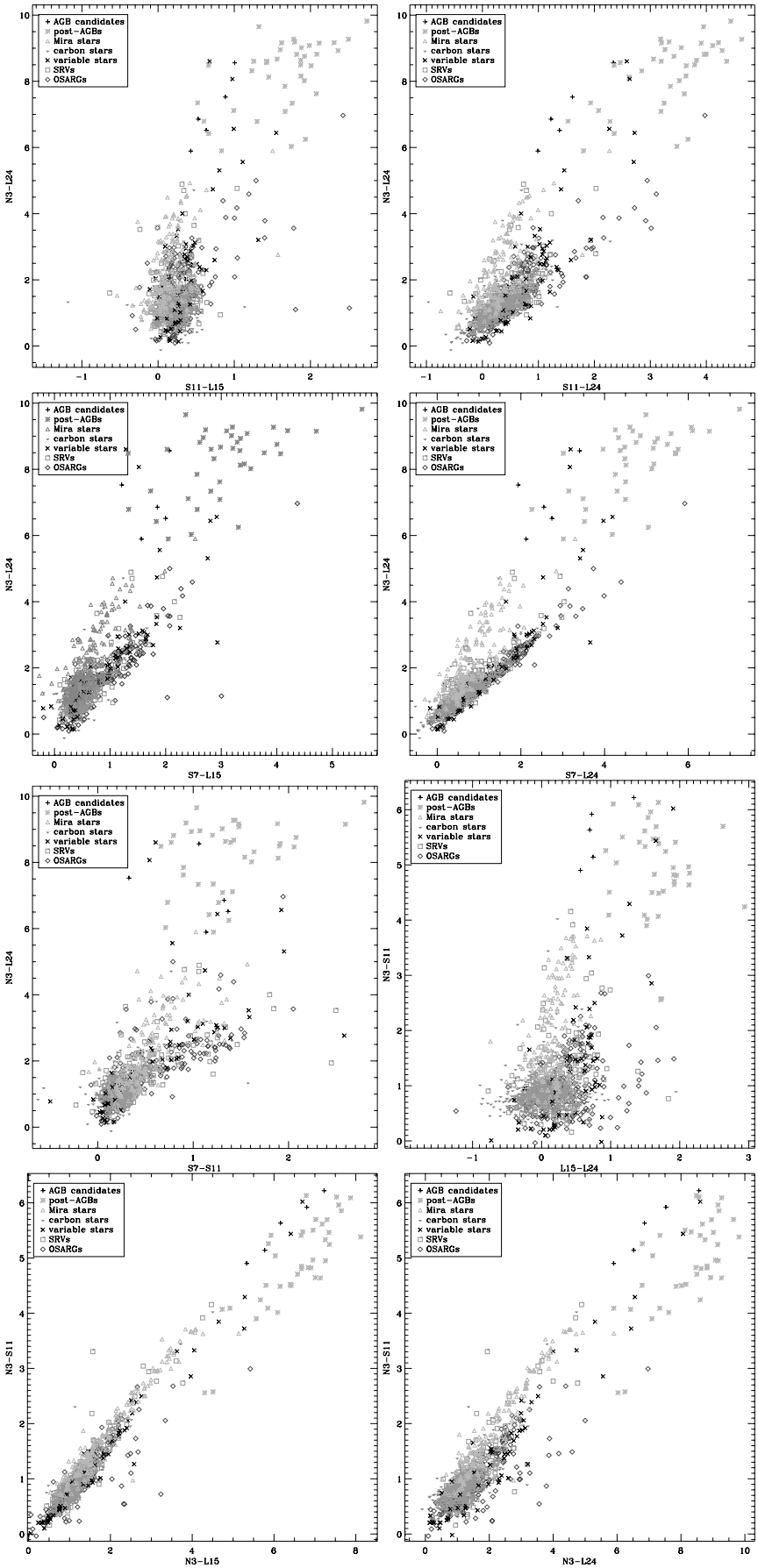

Fig. E.2. Position of AGB stars, late-type pulsating stars, possibly being AGBs or close to the AGB phase, and post-AGB stars in the color-color diagrams. All symbols as in Fig. 8.

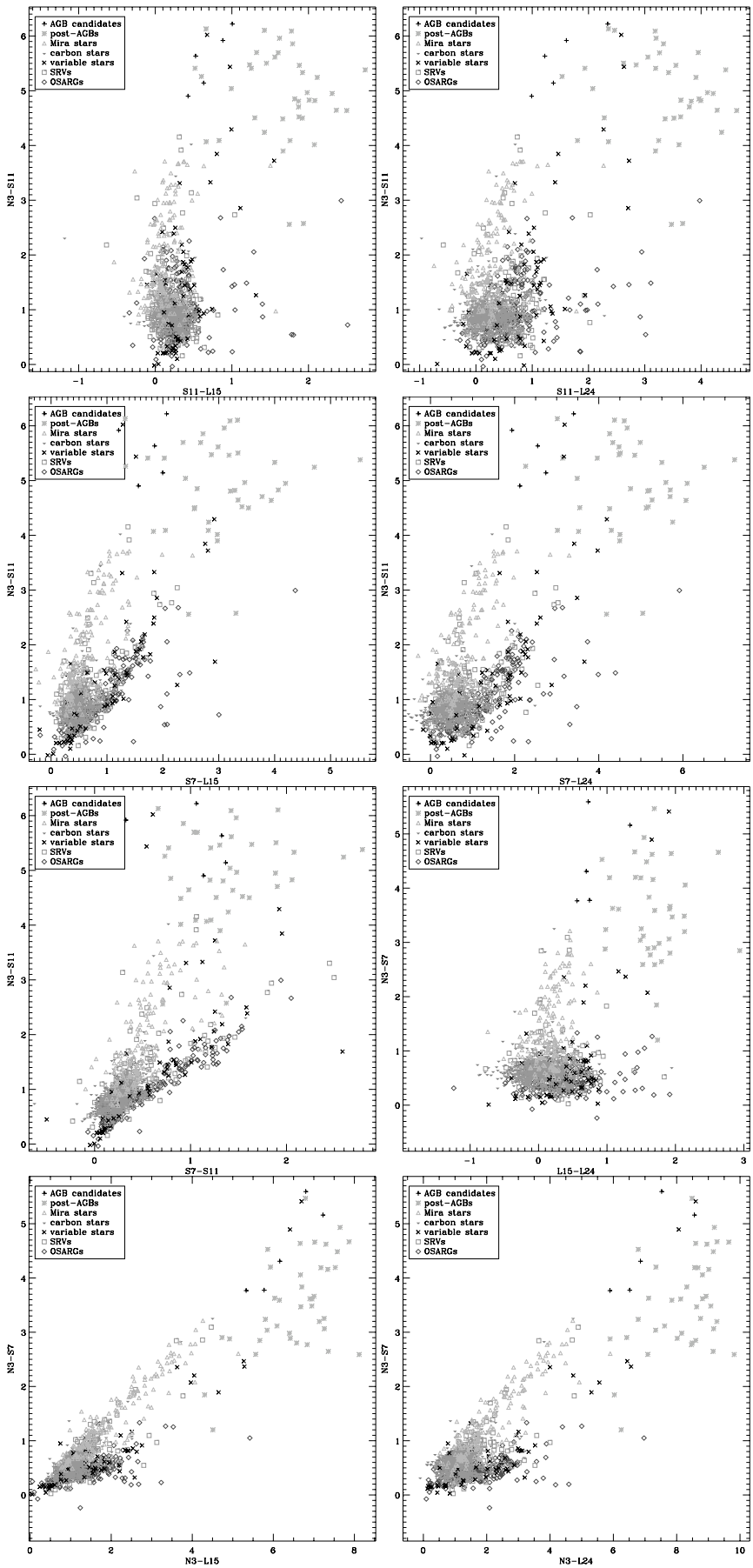

Fig. E.3. Position of AGB stars, late-type pulsating stars, possibly being AGBs or close to the AGB phase, and post-AGB stars in the color-color diagrams. All symbols as in Fig. 8.

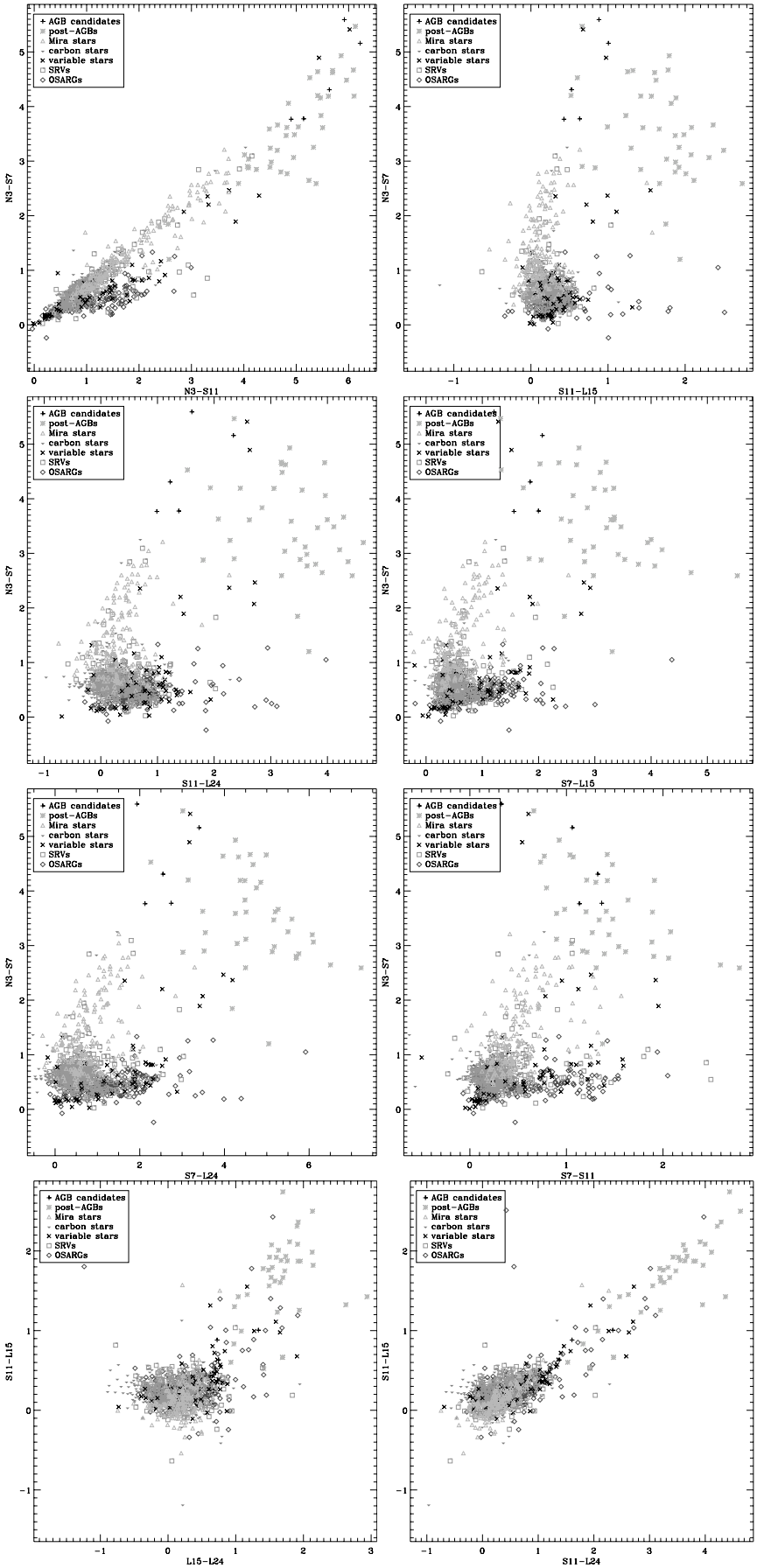

Fig. E.4. Position of AGB stars, late-type pulsating stars, possibly being AGBs or close to the AGB phase, and post-AGB stars in the color-color diagrams. All symbols as in Fig. 8.

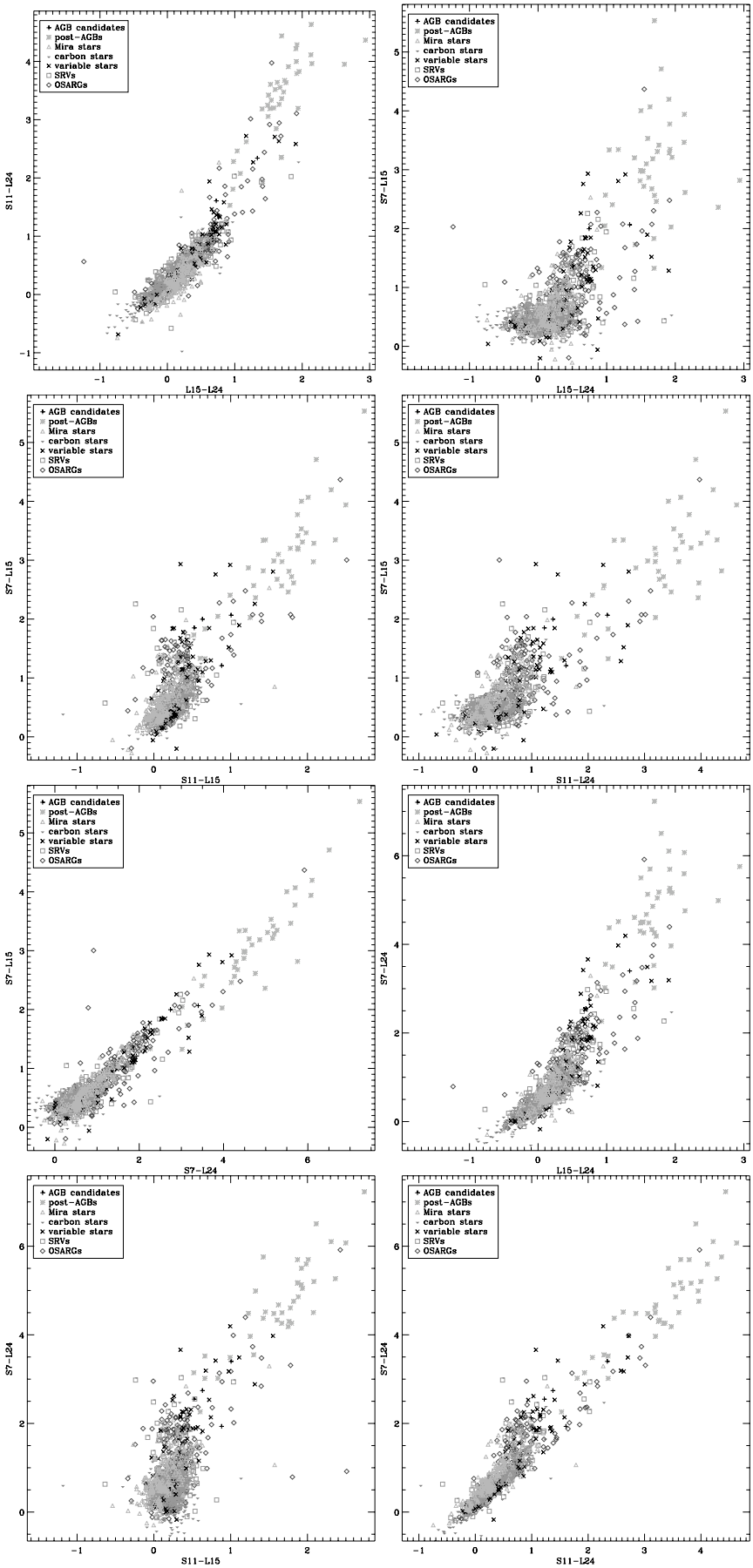

Fig. E.5. Position of AGB stars, late-type pulsating stars, possibly being AGBs or close to the AGB phase, and post-AGB stars in the color-color diagrams. All symbols as in Fig. 8.

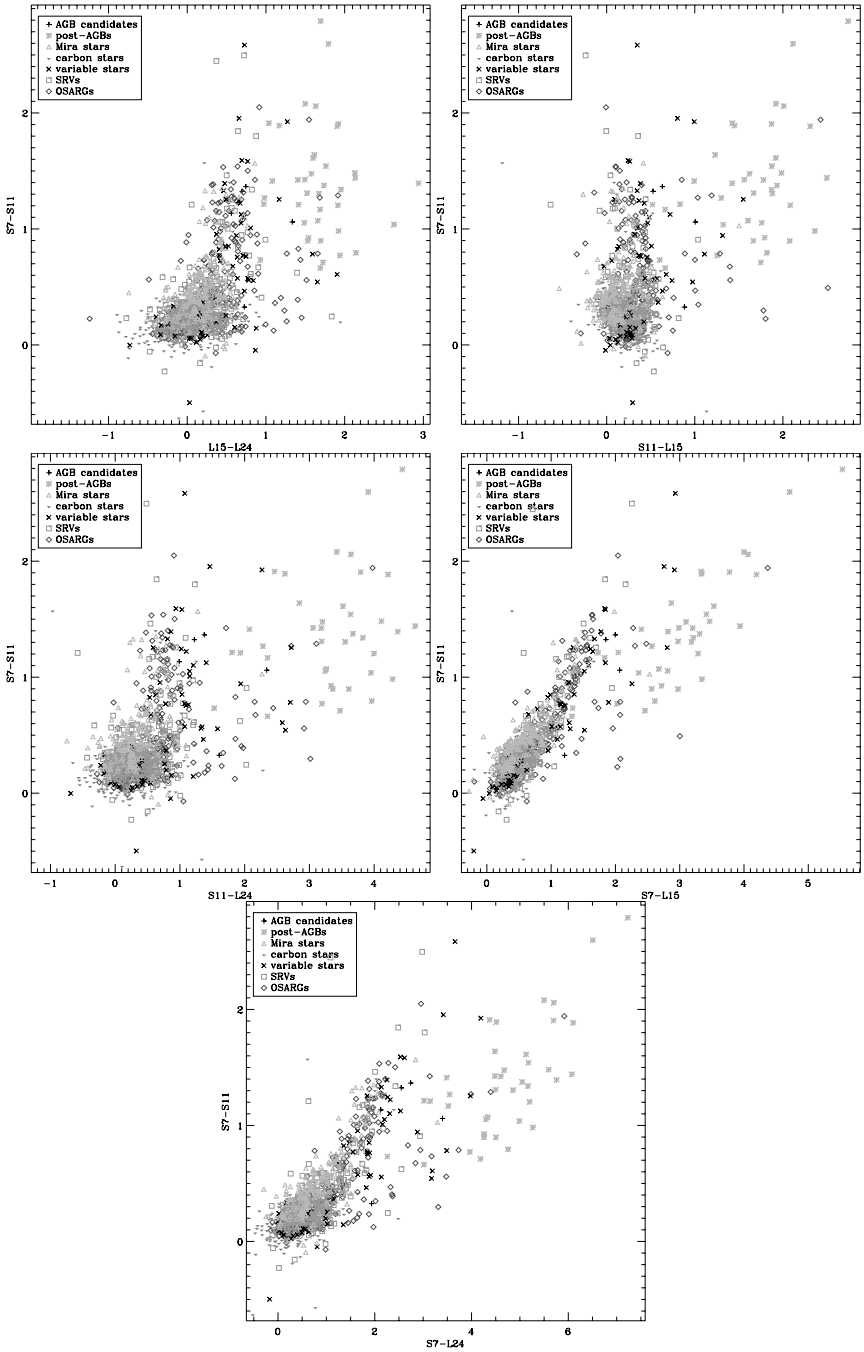

Fig. E.6. Position of AGB stars, late-type pulsating stars, possibly being AGBs or close to the AGB phase, and post-AGB stars in the color-color diagrams. All symbols as in Fig. 8.

Appendix F. Color-Magnitude Diagrams

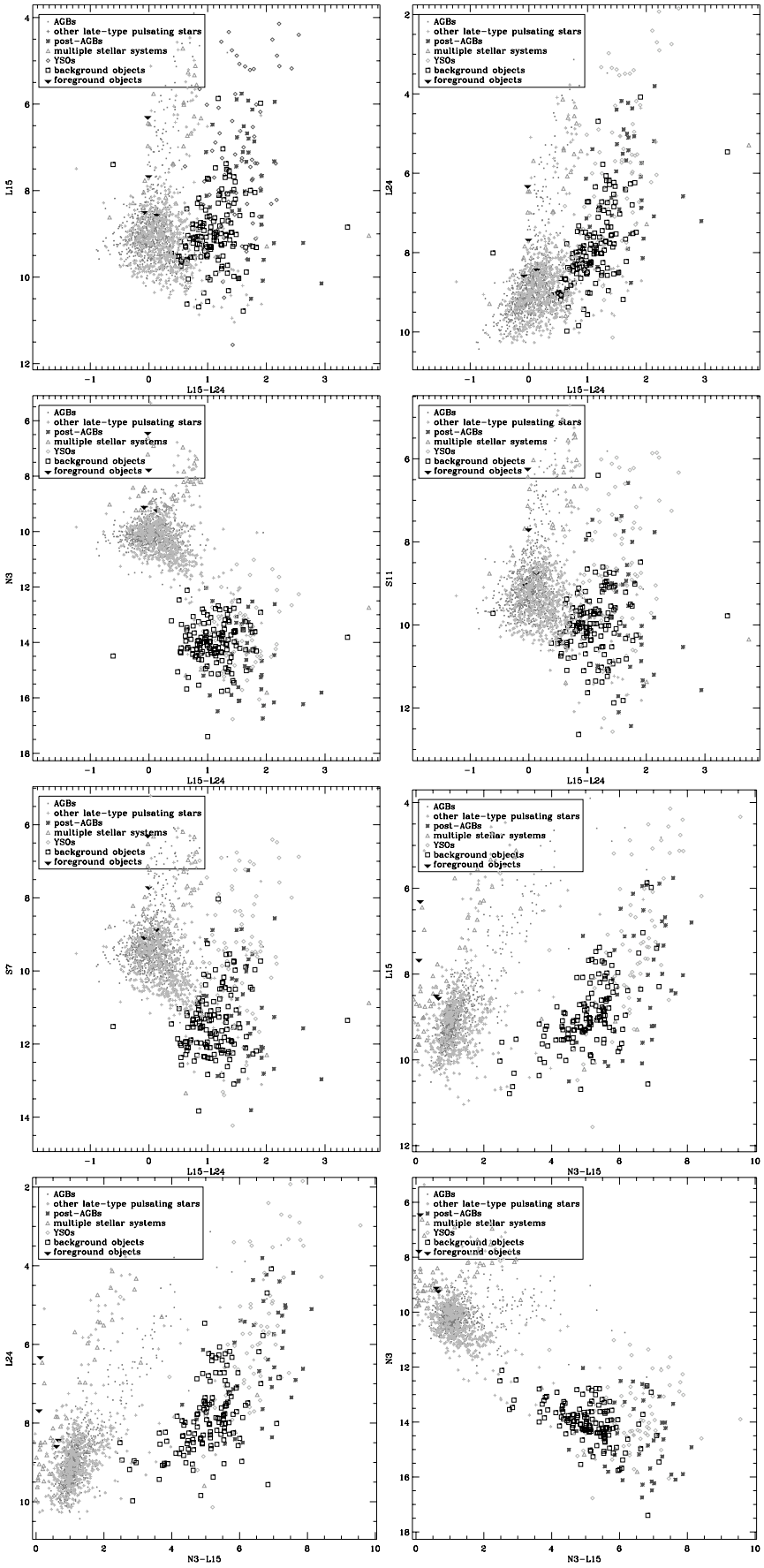

Fig. F.1. Position of different types of objects in the color-magnitude diagrams. All symbols as in Fig. 5.

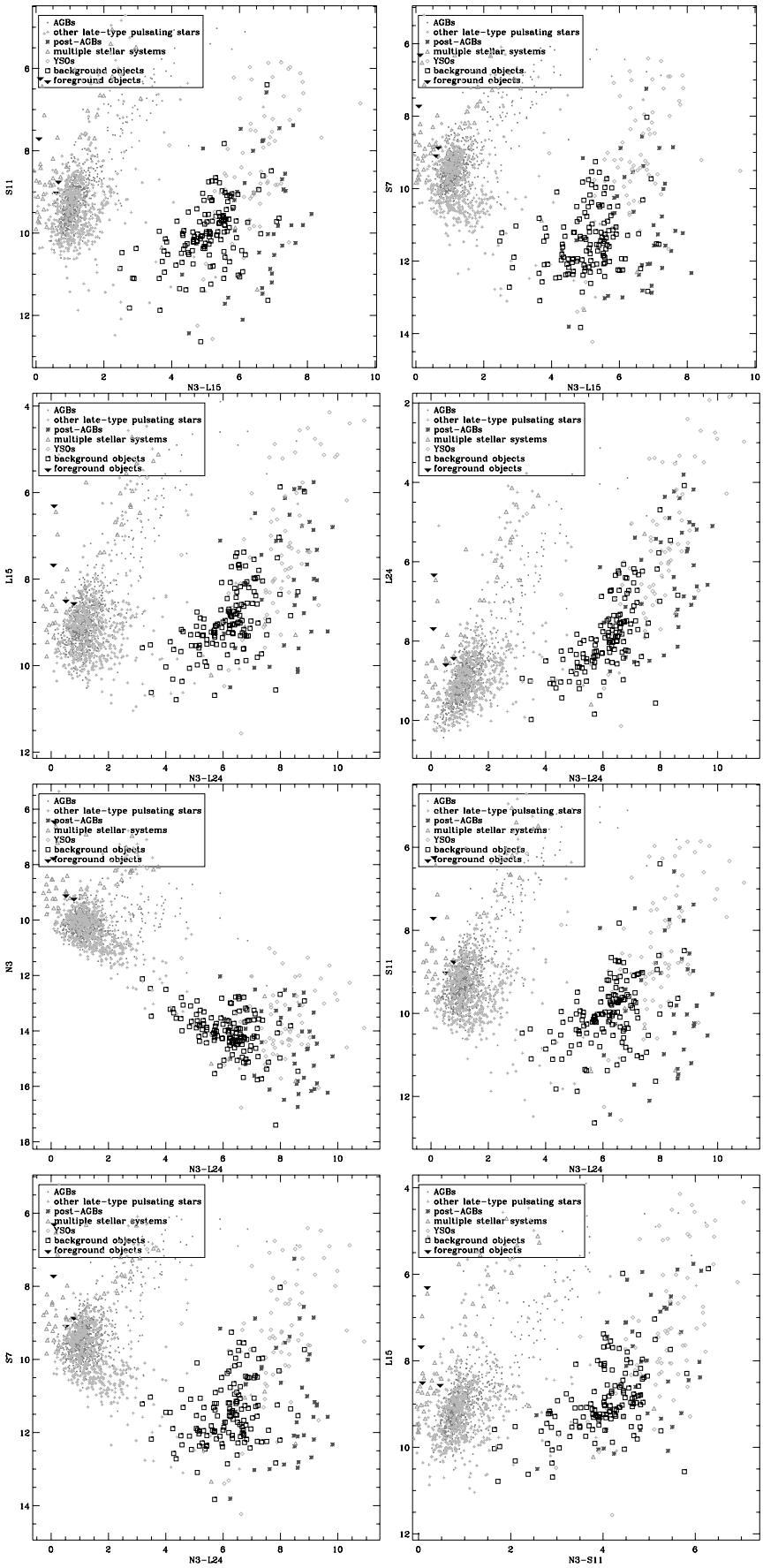

Fig. F.2. Position of different types of objects in the color-magnitude diagrams. All symbols as in Fig. 5.

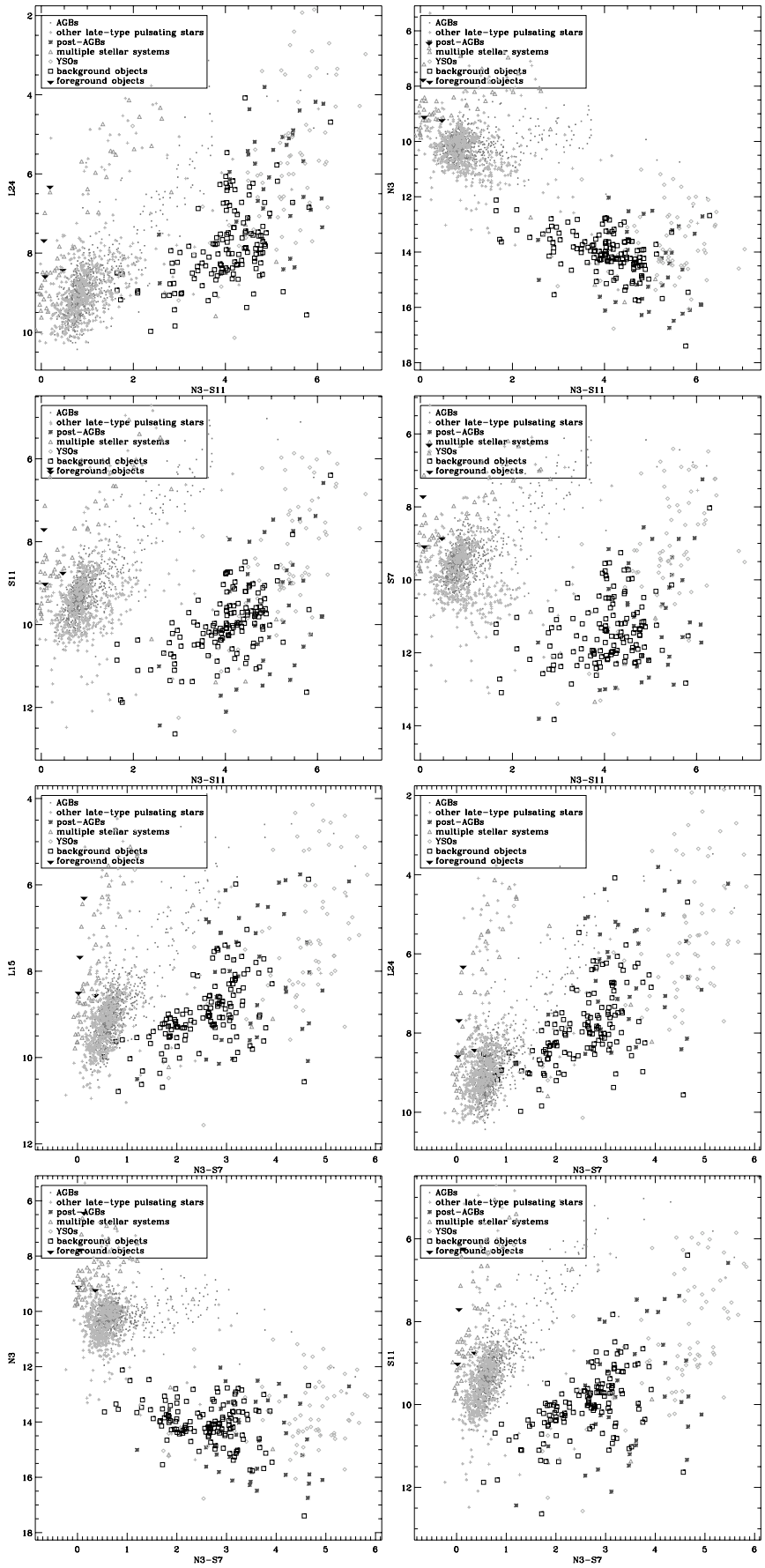

Fig. F.3. Position of different types of objects in the color-magnitude diagrams. All symbols as in Fig. 5.

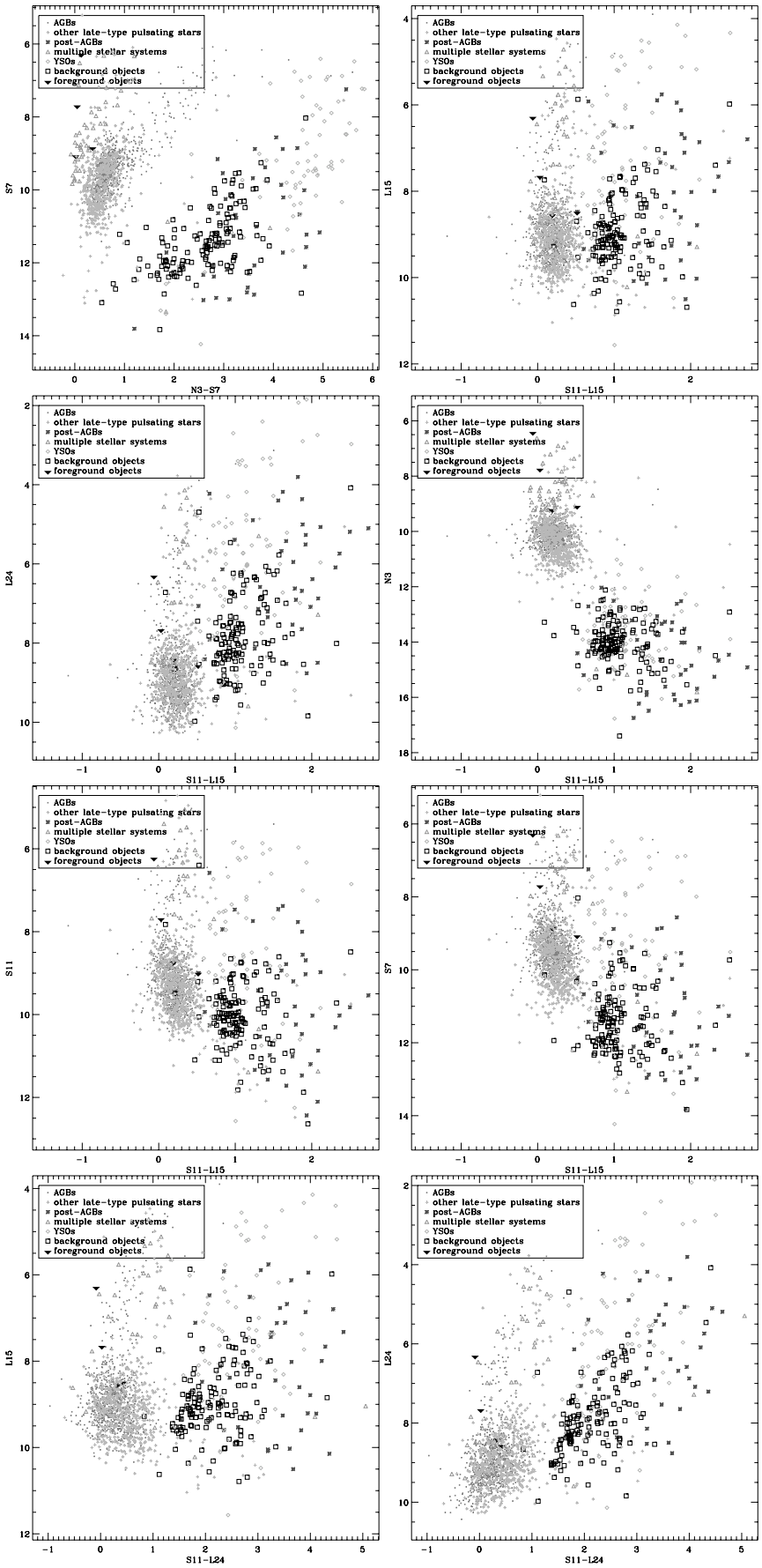

Fig. F.4. Position of different types of objects in the color-magnitude diagrams. All symbols as in Fig. 5.

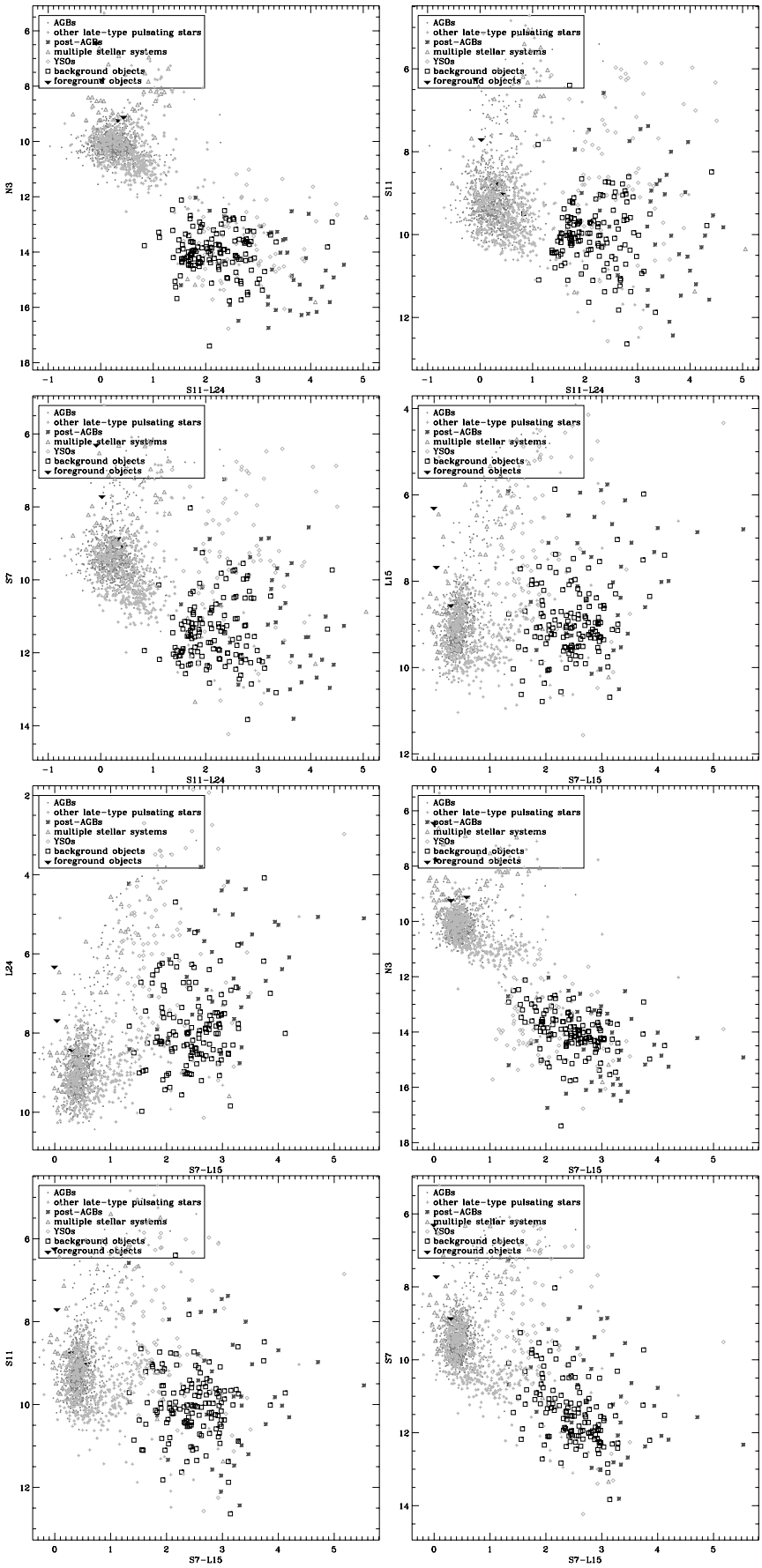

Fig. F.5. Position of different types of objects in the color-magnitude diagrams. All symbols as in Fig. 5.

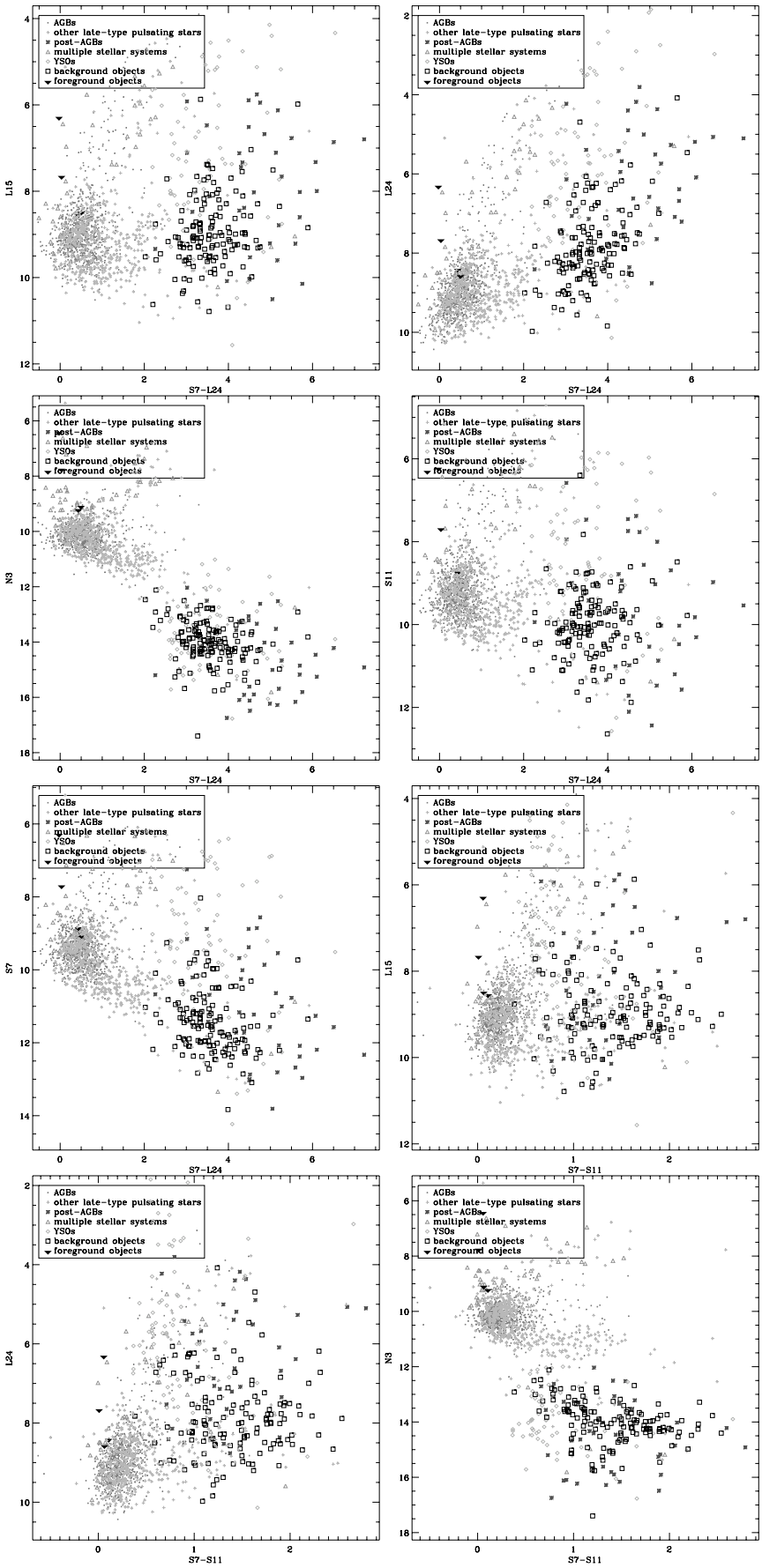

Fig. F.6. Position of different types of objects in the color-magnitude diagrams. All symbols as in Fig. 5.

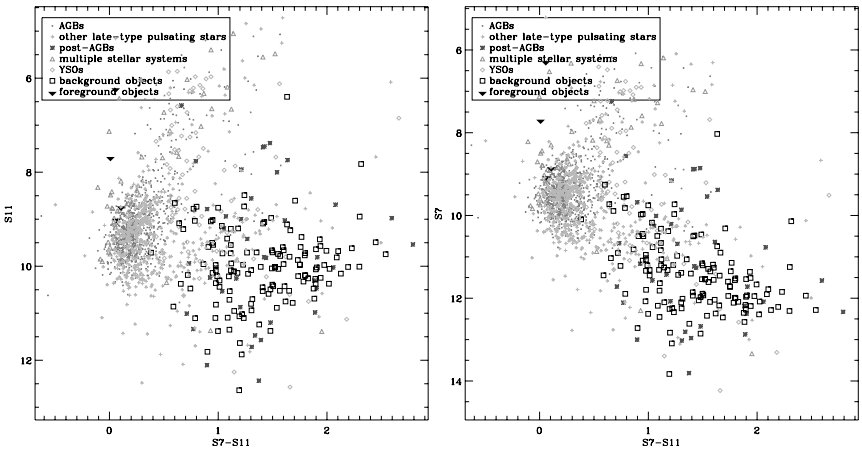

Fig. F.7. Position of different types of objects in the color-magnitude diagrams. All symbols as in Fig. 5.

Appendix G. Color-Magnitude Diagrams

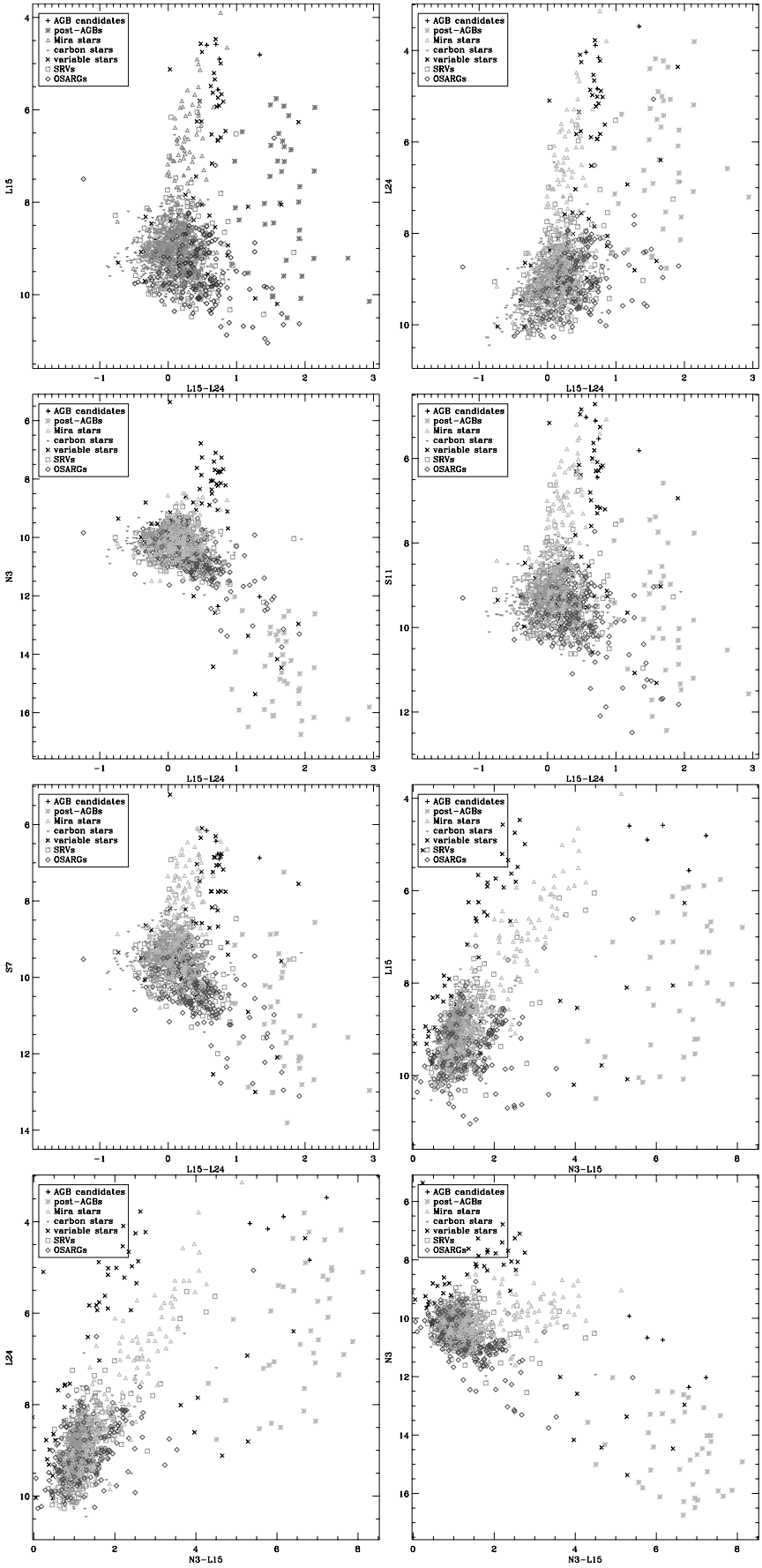

Fig. G.1. Position of AGB stars, late-type pulsating stars, possibly being AGBs or close to the AGB phase, and post-AGB stars in the color-color diagrams. All symbols as in Fig. 6.

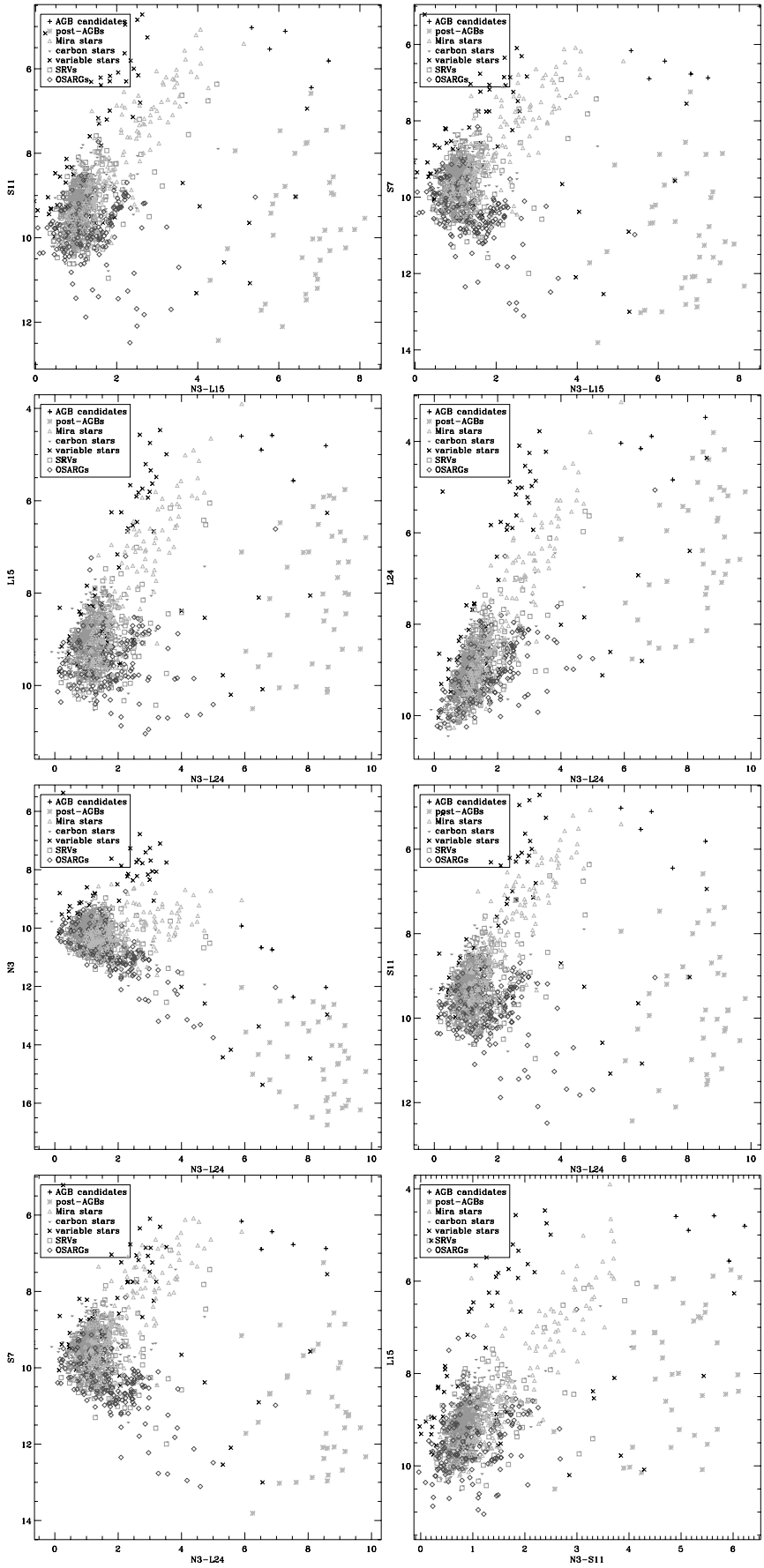

Fig. G.2. Position of AGB stars, late-type pulsating stars, possibly being AGBs or close to the AGB phase, and post-AGB stars in the color-color diagrams. All symbols as in Fig. 6.

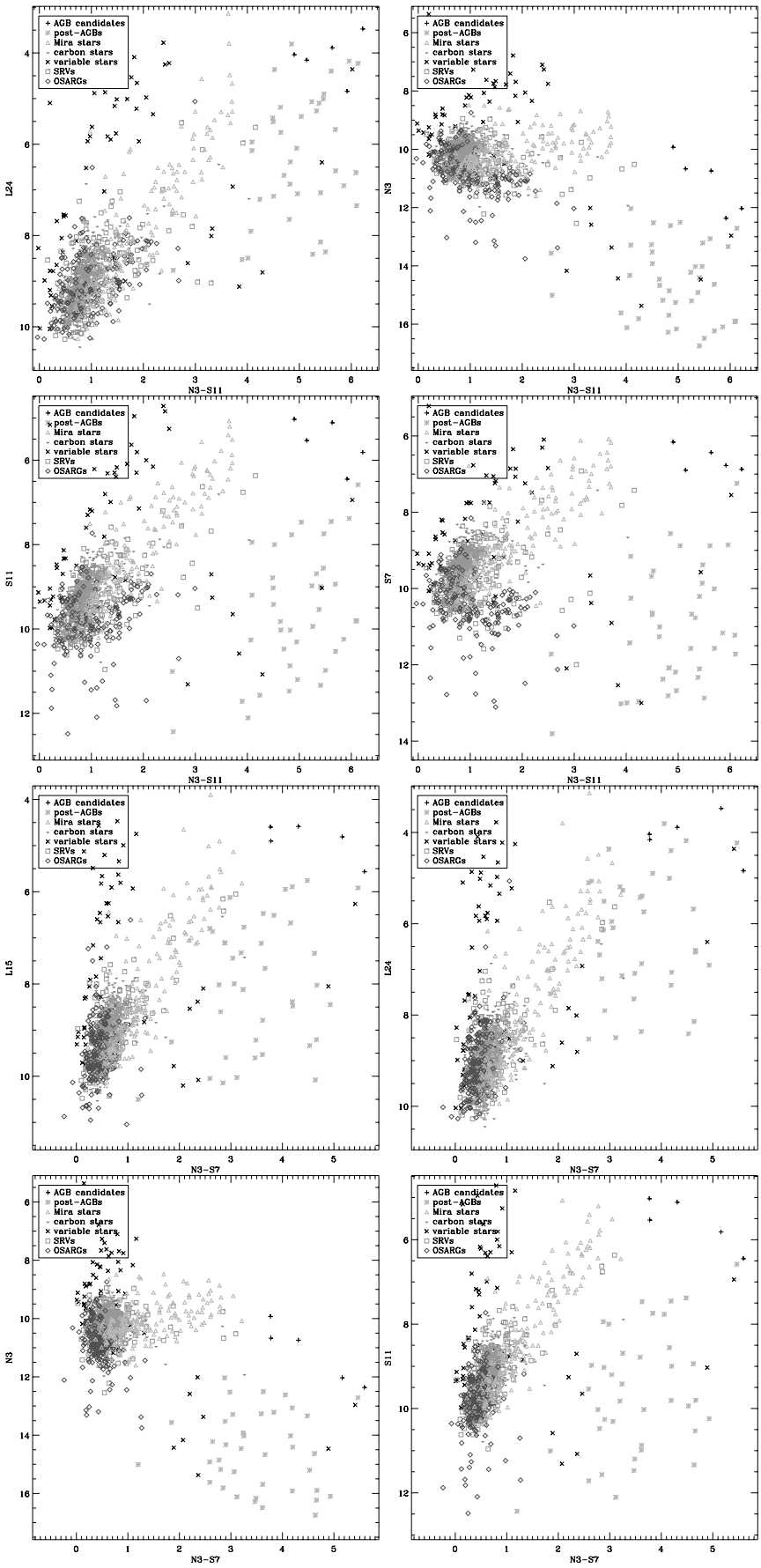

Fig. G.3. Position of AGB stars, late-type pulsating stars, possibly being AGBs or close to the AGB phase, and post-AGB stars in the color-color diagrams. All symbols as in Fig. 6.

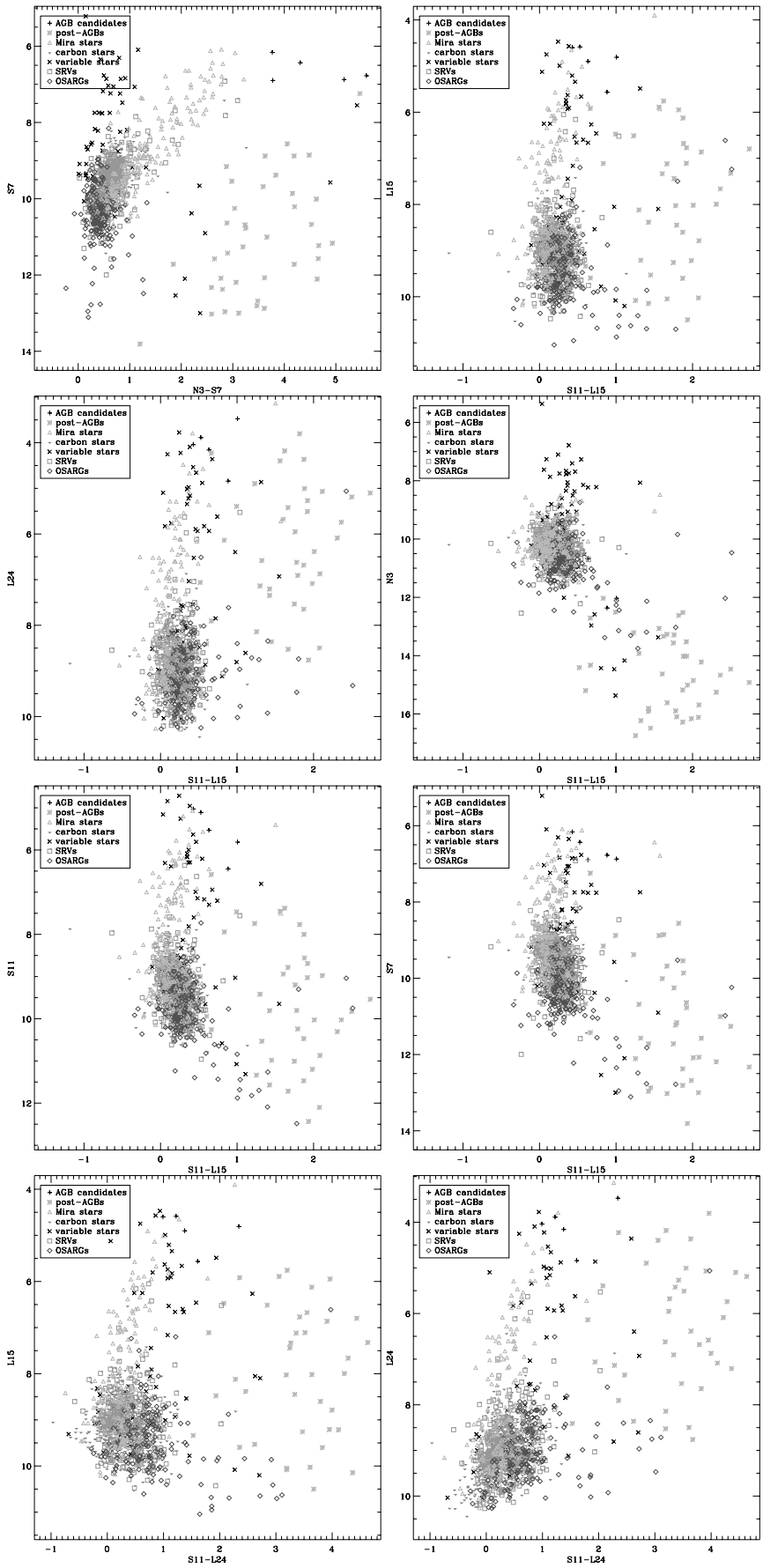

Fig. G.4. Position of AGB stars, late-type pulsating stars, possibly being AGBs or close to the AGB phase, and post-AGB stars in the color-color diagrams. All symbols as in Fig. 6.

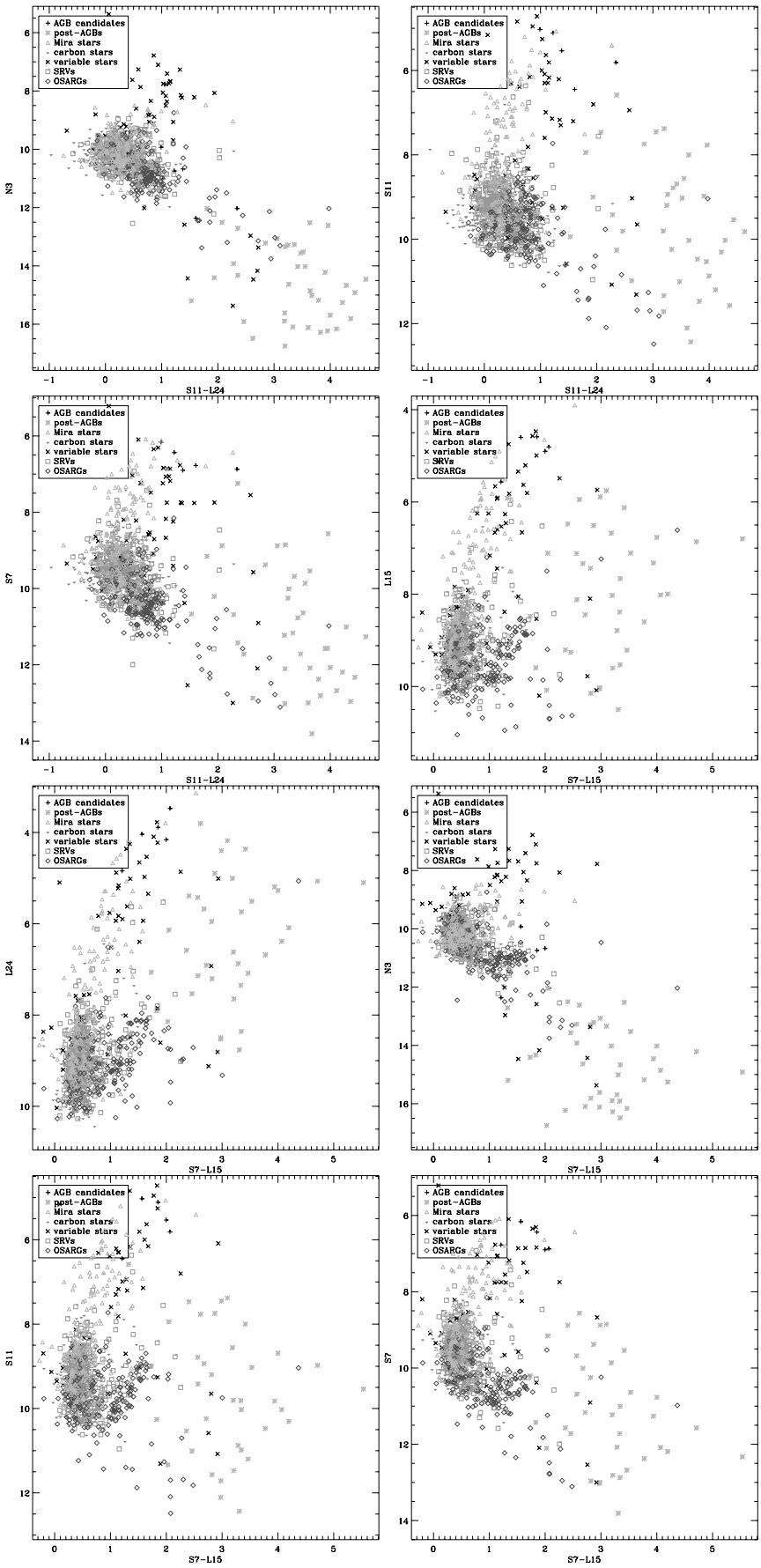

Fig. G.5. Position of AGB stars, late-type pulsating stars, possibly being AGBs or close to the AGB phase, and post-AGB stars in the color-color diagrams. All symbols as in Fig. 6.

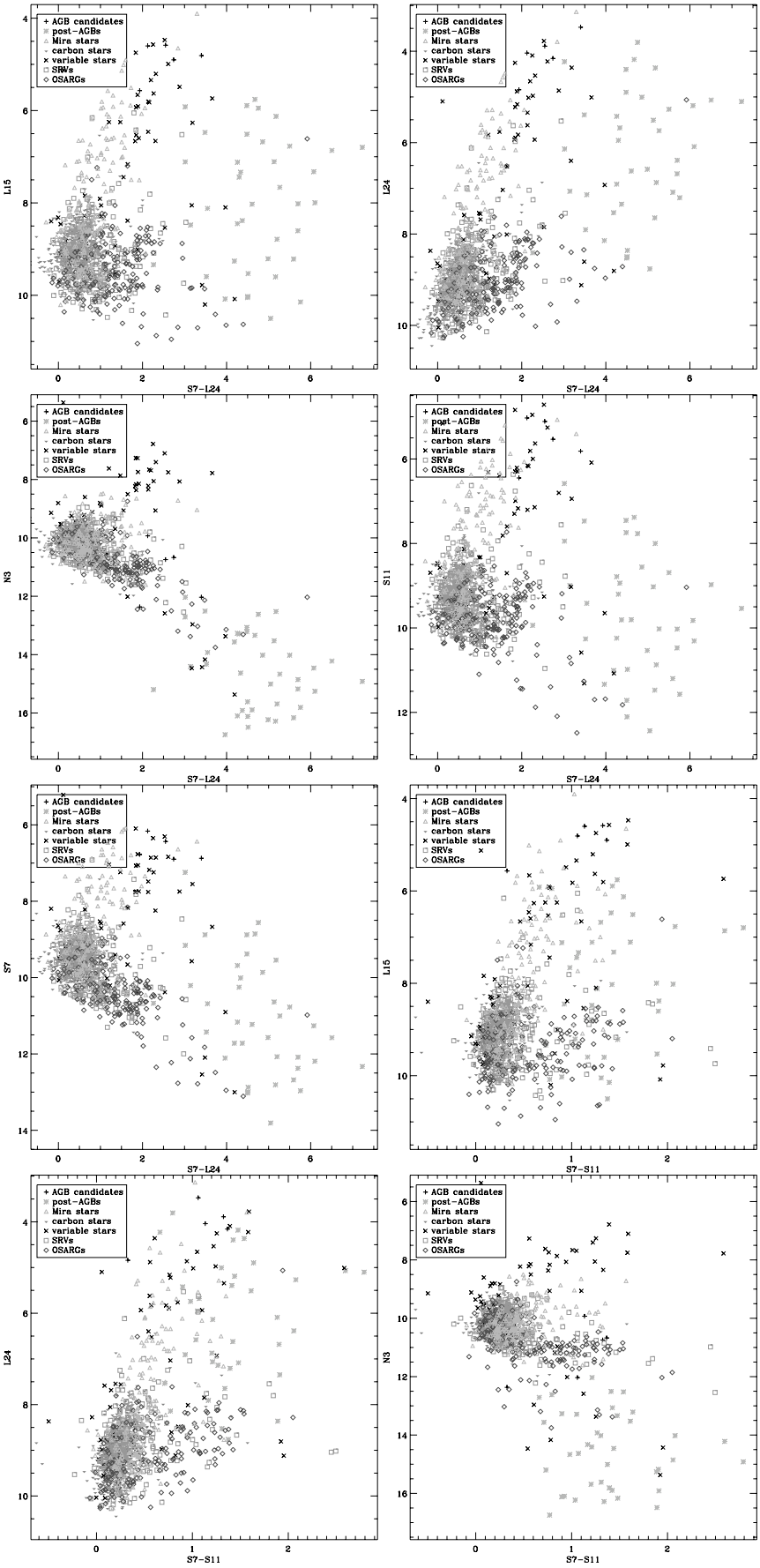

Fig. G.6. Position of AGB stars, late-type pulsating stars, possibly being AGBs or close to the AGB phase, and post-AGB stars in the color-color diagrams. All symbols as in Fig. 6.

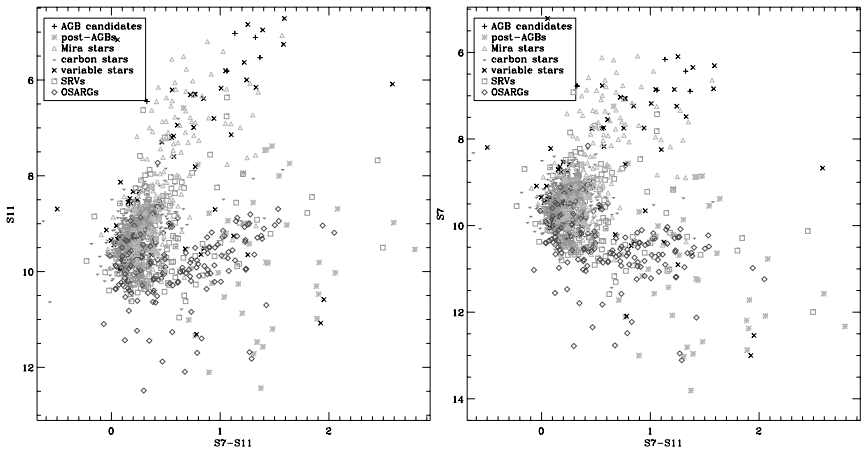

Fig. G.7. Position of AGB stars, late-type pulsating stars, possibly being AGBs or close to the AGB phase, and post-AGB stars in the color-color diagrams. All symbols as in Fig. 6.